Hindawi
Structural Control and Health Monitoring
Volume 2023, Article ID 3496666, 40 pages
https://doi.org/10.1155/2023/3496666

Research Article

An Adaptive Sparse Regularization Method for Response Covariance-Based Structural Damage Detection

Jian-Fu Lin,[1] **Wei-Lin Wu**,[1,2] **Jian-Liang Huang**,[2] **Jun-Fang Wang**,[3] **Wen-Xin Ren**,[3] **Yi-Qing Ni**,[4] **and Li-Xin Wang**[1]

[1]*Center of Safety Monitoring of Engineering Structures, Shenzhen Academy of Disaster Prevention and Reduction, China Earthquake Administration, Shenzhen 518003, China*
[2]*Department of Applied Mechanics and Engineering, School of Aeronautics and Astronautics, Sun Yat-Sen University, Shenzhen 518107, China*
[3]*MOE Key Laboratory for Resilient Infrastructures of Coastal Cities, College of Civil and Transportation Engineering, Shenzhen University, Shenzhen 518060, China*
[4]*Hong Kong Branch of National Rail Transit Electrification, Automation Engineering Technology Research Center, Department of Civil and Environmental Engineering, The Hong Kong Polytechnic University, Kowloon, Hong Kong, China*

Correspondence should be addressed to Jun-Fang Wang; jf.wang@szu.edu.cn

Received 24 September 2022; Revised 11 December 2022; Accepted 14 December 2022; Published 9 February 2023

Academic Editor: Jun Li

Structural damage detection is usually an ill-posed inverse problem due to the contamination of measurement noise and model error in structural health monitoring. To deal with the ill-posed damage detection problem, l_2-regularization is widely used. However, l_2-regularization tends to provide nonsparse solutions and distribute identified damage to many undamaged elements, potentially leading to false alarms. Therefore, an adaptive sparse regularization method is proposed, which considers spatially sparse damage as a prior constraint since structural damage often occurs in some locations with stiffness reduction at the sparse elements out of the large total number of elements in an entire structure. First, a response covariance-based convex cost function is established by incorporating an l_1-regularized term and an adaptive regularization factor to formulate the sparse regularization-based damage detection problem. Then, optimal sensor placement is conducted to determine the optimal measurement locations where the acceleration responses are adopted for computing the response covariance-based damage index and cost function. Further, the predictor-corrector primal-dual path-following approach, an efficient and robust convex optimization algorithm, is applied to search for solutions to the damage detection problem. Finally, a comparison study with the Tikhonov regularization-based damage detection method is conducted to examine the performance of the proposed adaptive sparse regularization-based method by using an overhanging beam model subjected to different damage scenarios and noise levels. The numerical study demonstrates that the proposed method can effectively and accurately identify damage under multiple damage scenarios with various noise levels, and it outperforms the Tikhonov regularization-based method in terms of high accuracy and few false alarms. The analyses on time consumption, adaptiveness of the sparse regularization factor, model-error resistance, and sensor number influence are conducted for further discussions of the proposed method.

1. Introduction

Structural degradation is inevitable in civil structures because they are subjected to complicated environments and extreme events in their service life. Structural degradation may threaten the functionality and safety of civil structures and even leads to catastrophic consequences. To ensure the safety of civil structures, structural damage detection is a cutting-edge technology developed in the past decades. Vibration-based damage detection methods have attracted much attention [1–15]. However, damage detection is usually an ill-posed inverse problem in structural health monitoring, and regularization methods play an important role in dealing with the ill-posed damage detection problem.

Tikhonov regularization (l_2-regularization) is a widely used regularization method for damage detection [16]. Titurus and Friswell [17] presented a sensitivity-based approach for integrating with Tikhonov regularization for model updating. Weber et al. [18] applied the Tikhonov regularization to a nonlinear structural damage problem. Li and Law [19] proposed an adaptive Tikhonov regularization method for damage detection, which could successfully identify damage locations and extents under considerable noise interruption. Zhu et al. [20] developed a sensitivity-based model updating approach for damage identification with unknown input excitation by adopting the Tikhonov regularization. An important reason for the wide application of Tikhonov regularization is that it has a closed-form solution and it is convenient to determine the regularization factor. However, the Tikhonov regularization tends to provide non-sparse solutions and distribute identified damage to many elements, thereby potentially resulting in false alarms.

Recently, l_1-regularization methods have attracted increasing interest in different aspects of structural health monitoring, including lost data recovery, load estimation, and damage detection [21, 22]. Especially many efforts have been devoted to the issue of l_1-regularization-based damage detection. Zhou et al. [23] investigated l_1-sparse-regularization-based structural damage detection, and the proposed method could effectively identify damage locations and extents in numerical studies in the condition with a small number of sensors, incomplete modal parameters, and measurement noise. Hernandez [24] minimized the incomplete spectrum-based cost function integrated with l_1-regularization for the damage detection of isolated structural damage of a beam model and a plane model. Zhou et al. [25] discussed the effects of the number of measurement data, damage severity, number of damages, and noise level on the l_1-regularization-based damage detection in the frequency domain. Wu and Zhou [26] and Hou et al. [27] applied an l_1-regularized model updating method to structural damage detection by taking advantage of modal frequencies and the combination of modal frequencies and mode shapes, and both numerical and experimental studies showed that the proposed method can reach more accurate results than the traditional l_2-regularized damage detection approach. Later, Hou et al. [28] employed the elastic net method, which combines l_1-and l_2-regularization to solve the damage detection problem, and it was demonstrated that either single or grouped damaged elements could be more effectively identified. Besides, Fan et al. [29] studied the sparse damage identification of piezoelectric ceramic by detecting resonance frequency shifts in the impedance. Further, Yue et al. [30] and Luo and Yu [31] have conducted comparative studies among different regularization strategies with l_p-norm constraints, for revealing the advantages of sparse regularization in damage detection. These studies mentioned above mainly used frequency-domain damage detection methods adopting natural frequencies or mode shapes as damage indexes. Although these methods do not require the measurement of excitations, modal parameters are often not sensitive enough to local damage because low-order modes are mainly used, while higher-order mode shapes are hard to obtain and sensitive to noise. Also, the extraction of completed mode shapes needs the installation of a large number of sensors, which is very difficult for a large structure. Alternatively, some other researchers integrated time-domain damage indexes with l_1-regularization for damage detection. Zhang and Xu [32] proposed an l_1-regularization-based damage detection method by directly using acceleration time history as a damage index, and both numerical and experimental studies have shown that the proposed approach could achieve more accurate results than the traditional l_2-regularized damage detection approach. Smith and Hernandez [33] presented an impulse response sensitivity-based approach enhanced by the LASSO algorithm to detect spatially sparse damage. Mountassir et al. [34] used ultrasonic response to detect damage in a steel tube based on sparse regularization. Chen et al. [35] proposed a novel l_1-regularization-based approach to identify the bridge influence line for damage identification.

For regularization-based damage detection methods, the regularization factor plays an important role to control the tradeoff between the data fidelity and solution size, and thus significantly influences the accuracy and stability of the solution. In contrast to the l_2-regularization-based methods, the suitable l_1-regularization factor is more difficult to obtain. Because there is no closed-form solution for the l_1-regularized problems, the regularization factor is generally acquired according to some empirical selection strategies. Mascarenas et al. [36] heuristically selected a fixed value of 1.0 as the l_1-regularization factor for compressed sensing data reconstruction in structural health monitoring. Yang and Nagarajaiah [37] adopted the l_1-regularized least-squares algorithm to solve the modal identification problem with the regularization parameter of 0.01, and the solution was not sensitive to the regularization parameter. Wang and Lu [38] proposed a threshold setting method to properly determine the sparse regularization parameter for a damage identification approach that combined the incomplete modal data with the sparse regularization. Zhang and Xu [32] developed a reweighted l_1-regularization method for enhancing the sparsity of solutions and alleviating the difficulty in choosing an appropriate regularization parameter. Lai and Nagarajaiah [39] employed the Akaike information criterion to determine the optimal sparse regularization factor for semi-supervised structural linear/nonlinear damage detection and characterization. Malioutov et al. [40] used the discrepancy principle to select a regularization factor in a sparse signal reconstruction study, and the factor was employed for matching the residue of the solution to some known statistics of noise. Hou et al. [41] discussed two feasible strategies to determine a sparse regularization parameter for l_1-regularized damage detection. The first one selects a compromised regularization parameter to ensure that both the residue and the solution are small enough, and the other one is based on the discrepancy principle, which requires that the variance of the discrepancy between the calculated and measured responses is close to the variance of the measurement noise. Yao et al. [42] attempted to select the regularization parameter based on the L-curve of data misfit versus model constraints for

localizing seismic sources, and it was realized by minimizing the l_2-norm of the difference between the observed and modeled waveforms penalized by the l_1-norm of the seismic source vector. Later, the L-curve criterion is similarly used to select a suitable regularization factor for some other l_1-regularization-based damage detection studies [30]. Moreover, the cross-validation algorithm was usually adopted to select the regularization factor for the elastic net-based damage detection method [28] and the LASSO regularization-based damage detection method [33]. Although there are various investigations on the selection strategies of the l_1-regularization factor, an adaptive regularization factor with a mathematical expression for automatic updating is rarely reported.

Therefore, this study aims at developing an adaptive sparse regularization-based damage detection method, which iteratively solves the damage identification results through the minimization of a new response covariance-based cost function incorporating an l_1-regularized term and an adaptive regularization factor. The methodology of the proposed adaptive sparse regularization-based structural damage detection is formulated in Section 2, and a procedure for implementing the proposed method is also described in this section. A comparison study is conducted in Section 3, where the proposed adaptive sparse regularization (ASR)-based and the Tikhonov regularization (TR)-based damage detection methods are comprehensively compared by using an overhanging beam model subjected to different levels of noise in different damage scenarios. In Section 4, the analyses on time consumption, adaptiveness of the sparse regularization factor, model-error resistance, and sensor number influence are conducted for further discussions of the proposed method. Finally, conclusions are drawn in Section 5.

2. Methodology

2.1. Inverse Problem in Damage Detection. The equation of motion of a linear-elastic damped structural system with N degrees-of-freedom (DOFs) can be written as follows:

$$\mathbf{M}\ddot{\mathbf{d}} + \mathbf{C}\dot{\mathbf{d}} + \mathbf{K}\mathbf{d} = \mathbf{L}_\mathbf{F}\mathbf{F}, \tag{1}$$

where $\mathbf{M}$, $\mathbf{C}$, and $\mathbf{K}$ are the mass, damping, and stiffness matrix, respectively; $\ddot{\mathbf{d}}$, $\dot{\mathbf{d}}$, and $\mathbf{d}$ are the acceleration, velocity, and displacement response vector, respectively; $\mathbf{F}$ is the excitation force vector; $\mathbf{L}_\mathbf{F}$ is the mapping matrix relating the excitation force to specific DOFs of the structure.

The response covariance-based damage index, which was proposed by Lin and Xu [7], is adopted in this paper. This time-domain index is effective for structural damage identification using a limited number of sensors, and it is sensitive to local damages and insensitive to measurement noise. The response covariance-based damage index vector $\mathbf{V}_{pq}$ can be expressed as follows:

$$\begin{aligned}\mathbf{V}_{pq} = \Big[&C_{p_1q_1}(\tau_0), C_{p_1q_2}(\tau_0), \cdots, C_{p_iq_j}(\tau_0), \cdots, C_{p_sq_s}(\tau_0), C_{p_1q_1}(\tau_1), C_{p_1q_2}(\tau_1), \cdots, C_{p_iq_j}(\tau_1), \cdots, C_{p_sq_s}(\tau_1), \cdots, C_{p_1q_1}(\tau_{nt-1}),\\ &C_{p_1q_2}(\tau_{nt-1}), \cdots, C_{p_iq_j}(\tau_{nt-1}), \cdots, C_{p_sq_s}(\tau_{nt-1})\Big]^T,\end{aligned} \tag{2}$$

with

$$C_{pq}(\tau) = \mathrm{E}[\hat{\ddot{\mathbf{d}}}p(t)\hat{\ddot{\mathbf{d}}}q(t+\tau)] = \mathrm{E}\left[\frac{\ddot{\mathbf{d}}p(t)}{\sigma_p^0}\frac{\ddot{\mathbf{d}}q(t+\tau)}{\sigma_q^0}\right], \tag{3}$$

where $C_{pq}(\tau)$ is the normalized cross-covariance function, and the subscript pq indicates that the function is calculated from responses recorded by the sensors p and q, respectively; $p_i \in [p_1, p_s]$ and $q_j \in [q_1, q_s]$, the subscript i or j denotes the i^{th} or the j^{th} sensor, and the subscript s denotes the total number of the sensors; $\hat{\ddot{\mathbf{d}}}_P(t)$ and $\hat{\ddot{\mathbf{d}}}_q(t)$ are the acceleration responses recorded by the sensors p and q; $\hat{\ddot{\mathbf{d}}}_P(t)$ and $\hat{\ddot{\mathbf{d}}}_q(t)$ with the hat $\hat{}$ represent the normalized acceleration responses; the normalized factors σ_p^0 and σ_q^0 are the standard deviations of $\hat{\ddot{\mathbf{d}}}_P$ and $\ddot{\mathbf{d}}_q$, respectively, and the superscript 0 denotes the response recorded from the intact structure; t is the time variable, τ is the time lag, and nt is the time lags number; the superscript T represents the operation of matrix transposition and $\mathrm{E}[\cdot]$ is the expectation operation. Since the acceleration responses have different orders of magnitude influenced by the excitation and sensor locations, they are normalized in equation (3) to relieve the ill-posed problem in the subsequent damage detection.

With local structural damages assumed as linear stiffness reduction happening to specific elements of the structure, the global stiffness matrix for the structure's damage state is expressed as the sum of element stiffness matrixes in the following:

$$\mathbf{K}^d = \sum_{i=1}^{\mathrm{ne}} \alpha_i \mathbf{K}_i = \sum_{i=1}^{\mathrm{ne}} (1 + \Delta\alpha_i)\mathbf{K}_i;\ (0 \le \alpha_i \le 1, -1 \le \Delta\alpha_i \le 0), \tag{4}$$

where $\mathbf{K}^d$ and $\mathbf{K}_i$ are the global stiffness matrix of the damaged structure and the element stiffness matrix of the i^{th} element, respectively, and the superscript d of $\mathbf{K}^d$ denotes the damaged state for the global stiffness matrix; $\alpha_i \in \alpha$ is the coefficient of stiffness matrix corresponding to the i^{th} element; $\Delta\alpha_i \in \Delta\alpha$ is the fractional change in stiffness of the i^{th}

element; the notation α denotes a vector of the coefficients of the stiffness matrix; $\Delta\alpha$ denotes the vector of the total fractional stiffness change in the damage elements; ne denotes the total element number of the structure.

A sensitivity-based damage detection approach is employed by cooperating with the response covariance index vector. The measured response covariance-based damage index vector $\mathbf{V}_{pq}^{m}$ is obtained from the measured responses by using equation (2), in which the superscript m and the subscript pq denote that the index vector is computed by using the measurement responses recorded by the sensors p and q. The measured damage index vector $\mathbf{V}_{pq}^{m}$ can be expressed in a first-order Taylor expansion as follows:

$$\mathbf{V}_{pq}^{\mathrm{m}} \approx \mathbf{V}_{pq}^{\mathrm{c}} + \frac{\partial \mathbf{V}_{pq}^{c}}{\partial \boldsymbol{\alpha}} \Delta\boldsymbol{\alpha}, \tag{5}$$

where $\mathbf{V}_{pq}^{c}$ is the computed response covariance-based damage index vector, in which the superscript c and the subscript pq denote that the index vector is computed by using the calculated responses of the sensors p and q from the finite element (FE) model. Equation (5) can be further rewritten as equation (6), which is a linear damage detection equation integrated with the iterative Gaussian–Newton algorithm.

$$\Delta\mathbf{V}_{pq}^{k} \approx \mathbf{S}^{k}\Delta\boldsymbol{\alpha}^{k+1};\ (k = 0, 1, 2\cdots), \tag{6}$$

with

$$\Delta\mathbf{V}_{pq} = \mathbf{V}_{pq}^{m} - \mathbf{V}_{pq}^{c}, \tag{7}$$

$$\mathbf{S} = \frac{\partial \mathbf{V}_{pq}^{c}}{\partial \boldsymbol{\alpha}} = \left[\frac{\partial \mathbf{V}_{pq}^{c}}{\partial \alpha_1}, \frac{\partial \mathbf{V}_{pq}^{c}}{\partial \alpha_2}, \cdots, \frac{\partial \mathbf{V}_{pq}^{c}}{\partial \alpha_i}, \cdots, \frac{\partial \mathbf{V}_{pq}^{c}}{\partial \alpha_{\mathrm{ne}}}\right], \tag{8}$$

where $\Delta\mathbf{V}_{pq}$ is the difference between $\mathbf{V}_{pq}^{m}$ and $\mathbf{V}_{pq}^{c}$; $\mathbf{S}$ is the sensitivity matrix of the damage index vector to the fractional stiffness change vector $\Delta\alpha$, which can be obtained by using the finite difference method; the superscript k denotes the iteration number; $\Delta\boldsymbol{\alpha}^{k+1}$ is the fractional stiffness change obtained at the $(k+1)^{\mathrm{th}}$ iteration.

The damage detection by directly solving equation (6) is generally an ill-posed inverse problem, and thus it is transformed into the following minimization optimization problem solved by the Tikhonov regularization method [16].

$$\begin{aligned}\Delta\boldsymbol{\alpha}^{k+1} = \underset{\Delta\boldsymbol{\alpha}^{k+1}}{\operatorname{argmin}} J\left(\Delta\boldsymbol{\alpha}^{k+1}, \lambda^{k+1}\right) = \underset{\Delta\boldsymbol{\alpha}^{k+1}}{\operatorname{argmin}}\left[\left\|\mathbf{S}^{k}\Delta\boldsymbol{\alpha}^{k+1} - \Delta\mathbf{V}_{pq}^{k}\right\|_2 + \lambda^{k+1}\left\|\Delta\boldsymbol{\alpha}^{k+1}\right\|_2\right],\\ \text{s.t.} -1 \le \Delta\alpha_i^{k+1} + \sum\Delta\alpha_i^{k} \le 0;\ \lambda^{k+1} \ge 0,\end{aligned} \tag{9}$$

where $\Delta\boldsymbol{\alpha}^{k+1}$ is gradually calculated at each iteration; the regularization factor λ^{k+1} can be obtained by using the L-curve criterion [16]. The accumulated stiffness reduction vector $\Delta\alpha$ in equation (5) can be finally obtained by $\Delta\alpha = \sum\Delta\boldsymbol{\alpha}^{k+1}$. Thereafter, the corresponding locations and severities of damage are consequently identified and embodied by $\Delta\boldsymbol{\alpha}$, in which $\Delta\boldsymbol{\alpha}_i = \sum\Delta\boldsymbol{\alpha}_i^{k+1}$ indicates the damage severity of the i^{th} element.

2.2. Adaptive Sparse Regularization for Damage Detection. Considering the sparsity of the structural damage, a new convex cost function with sparse regularization is proposed to not only stabilize the ill-posed problem but also enforce sparsity in the solution. By replacing the l_2-regularized term and the regularization factor λ in equation (9) with a new l_1-regularized term and an adaptive regularization factor, the new cost function can be explicitly expressed as follows:

$$J\left(\Delta\boldsymbol{\alpha}^{k+1}, \lambda^{*k+1}\right) = \left\|\mathbf{S}^{k}\Delta\boldsymbol{\alpha}^{k+1} - \Delta\mathbf{V}_{pq}^{k}\right\|_2 + \lambda^{*k+1}\left\|\sum\Delta\boldsymbol{\alpha}^{k+1}\right\|_1, \tag{10}$$

where the sparse regularization term $\|\sum\Delta\boldsymbol{\alpha}^{k+1}\|_1$ is the l_1-norm of the accumulated stiffness reduction vector of the $k+1$ iterations, and the λ^{*k+1} with the superscript $*$ denotes the adaptive regularization factor of the $(k+1)^{\mathrm{th}}$ iteration. The accumulated stiffness reduction $\Delta\boldsymbol{\alpha} = \sum\Delta\boldsymbol{\alpha}^{k+1}$, rather than a one-step adjustment in stiffness reduction $\Delta\boldsymbol{\alpha}^{k+1}$, represents structural damage locations and severities. Therefore, the sparse constraint on the accumulated stiffness reduction enables the constraint to accord closely with the fact that the spatial distribution of local damages is generally sparse. Meanwhile, this indirectly loosens the constraint on each one-step adjustment in stiffness reduction during the model updating process and thus facilitates more flexible adjustment of one-step stiffness reduction. In other words, proposing the use of the accumulated stiffness reduction in the sparse regularization term enhances both the sparsity of the final solution and the flexibility of one-step adjustment, which is potentially beneficial to the improvement of damage detection performance.

The fractional stiffness change $\Delta\boldsymbol{\alpha}^{k+1}$ at each iteration can be calculated by minimizing the cost function described by equation (10), and it is expressed as follows:

$$\Delta\boldsymbol{\alpha}^{k+1} = \underset{\Delta\boldsymbol{\alpha}^{k+1}}{\operatorname{argmin}} J\left(\Delta\boldsymbol{\alpha}^{k+1}, \lambda^{*k+1}\right) = \underset{\Delta\boldsymbol{\alpha}^{k+1}}{\operatorname{argmin}}\left[\left\|\mathbf{S}^{k}\Delta\boldsymbol{\alpha}^{k+1} - \Delta\mathbf{V}_{pq}^{k}\right\|_2 + \lambda^{*k+1}\left\|\sum\Delta\boldsymbol{\alpha}^{k+1}\right\|_1\right], \quad \text{s.t.} -1 \le \Delta\alpha_i^{k+1} + \sum\Delta\alpha_i^{k} \le 0; \lambda^{*k+1} \ge 0, \tag{11}$$

Generally, there is no closed-form solution for the l_1-regularization, and thus the damage detection problem in equation (11) is searched by using a convex optimization algorithm. The predictor-corrector primal-dual path-following approach, an efficient and robust semidefinite programming algorithm SDPT3 [43], is employed to solve equation (11). However, different from the l_2-regularization method, the existing l_1-regularization factor is often set according to subjective or empirical selection strategies without an analytic or adaptive expression. To conquer the obstacle of acquiring a suitable l_1-regularization factor, an adaptive regularization factor λ^{*k+1} with mathematical expression is proposed and formulated as follows:

$$\lambda^{*k+1} = \frac{\left\|\mathbf{S}^{k}\Delta\boldsymbol{\alpha}^{k+1} - \Delta\mathbf{V}_{pq}^{k}\right\|_2}{\left\|\sum\Delta\boldsymbol{\alpha}^{k+1}\right\|_1} \approx \frac{\left\|\mathbf{S}^{k}\Delta\boldsymbol{\alpha}_{\mathrm{r}}^{k+1} - \Delta\mathbf{V}_{pq}^{k}\right\|_2}{\left\|\sum(\Delta\boldsymbol{\alpha}^{k}) + \Delta\boldsymbol{\alpha}_{\mathrm{r}}^{k+1}\right\|_1}, \tag{12}$$

with

$$\Delta\boldsymbol{\alpha}_{\mathrm{r}}^{k+1} = \underset{\Delta\boldsymbol{\alpha}_{\mathrm{r}}^{k+1}}{\operatorname{argmin}}\left[\left\|\mathbf{S}^{k}\Delta\boldsymbol{\alpha}_{\mathrm{r}}^{k+1} - \Delta\mathbf{V}_{pq}^{k}\right\|_2\right], \tag{13}$$

where $\Delta\alpha_{\mathrm{r}}^{k+1}$ is the estimated stiffness reduction at the $(k+1)^{\mathrm{th}}$ iteration for calculating the adaptive regularization factor λ^{*k+1}, and the subscript r denotes that the estimated stiffness reduction is a reference value for the stiffness reduction at the $(k+1)^{\mathrm{th}}$ iteration; $\sum(\Delta\boldsymbol{\alpha}^{k})$ is the accumulated stiffness reduction vector of the previous k iterations.

The residue norm $\|\mathbf{S}^{k}\Delta\boldsymbol{\alpha}^{k+1} - \Delta\mathbf{V}_{pq}^{k}\|_2$ evaluates the data fidelity, and the solution norm $\|\sum\Delta\boldsymbol{\alpha}^{k+1}\|_1$ indicates the sparsity of the solution in equation (11), and both are important constraints for accurate damage detection. A suitable adaptive regularization factor is crucial for controlling the tradeoff between the l_2-norm of the residue and the l_1-norm of the solution. A too-small regularization factor will place high weighting on the residue norm and may result in an overfitting solution contaminated by measurement noise or model error, while a too-large regularization factor means that the solution norm becomes extra dominant, and this may lead to an oversmoothed solution. Therefore, the proposed adaptive regularization factor λ^{*k+1} is derived by assuming that the contributions of the residue norm and solution norm are equally important for achieving an accurate and sparse solution, that is, $\|\mathbf{S}^{k}\Delta\boldsymbol{\alpha}^{k+1} - \Delta\mathbf{V}_{pq}^{k}\|_2 = \lambda^{*k+1}\|\sum\Delta\boldsymbol{\alpha}^{k+1}\|_1$. As the $\Delta\boldsymbol{\alpha}^{k+1}$ is unknown before solving the optimization problem in equation (11), the adaptive regularization factor in equation (12) is alternatively estimated by using an approximate value of $\Delta\boldsymbol{\alpha}^{k+1}$, i.e., $\sum(\Delta\boldsymbol{\alpha}^{k}) + \Delta\boldsymbol{\alpha}_{\mathrm{r}}^{k+1}$. The $\Delta\boldsymbol{\alpha}_{\mathrm{r}}^{k+1}$ is estimated by solving equation (13) through the SDPT3 algorithm. Then, an appropriate λ^{*k+1} can be calculated by using equation (12) at each iteration before substituting λ^{*k+1} into equation (11) and conducting the $(k+1)^{\mathrm{th}}$ solving process of this equation. For each iteration, the λ^{*k+1} is automatically updated to keep the balance between the data fidelity and sparsity of the solution.

2.3. Procedure of the Adaptive Sparse Regularization-Based Damage Detection. The detailed implementation procedure of the proposed adaptive sparse regularization-based damage detection integrated with optimal sensor placement is depicted in Figure 1 and described as follows:

Step 1. Establish the FE model and initialize the model state: the initial iteration number $k = 0$, the initial stiffness reduction factor $\Delta\boldsymbol{\alpha}^{0}$ is filled with a zero vector $\mathbf{O}^{\mathrm{ne}\times 1}$ ($\Delta\boldsymbol{\alpha}^{0} = \mathbf{O}^{\mathrm{ne}\times 1}$), and the initial sensitivity matrix is set as $\mathbf{S}^{0} = \mathbf{S}(\Delta\boldsymbol{\alpha}^{0})$.

Step 2. Based on the established FE model, the effective-independence (EfI) [44] optimal sensor placement is conducted before the damage detection study. Specifically, set the target sensor number and establish the candidate location list initially. Then, the mode shape matrix $\boldsymbol{\Phi}$ of the current candidate locations is computed through modal analysis of the intact FE model, and the independence contribution vector $\mathbf{EI} = \mathrm{diag}[\boldsymbol{\Phi}(\boldsymbol{\Phi}^{\mathrm{T}}\boldsymbol{\Phi})^{-1}\boldsymbol{\Phi}^{\mathrm{T}}]$ is computed from the current candidate list. Thereafter, remove the candidate location with the minimum contribution to the modal independence from the candidate list and the mode shape matrix $\boldsymbol{\Phi}$. The process of calculating $\mathbf{EI}$ and removing candidate locations is repeated until the candidate location number is reduced to the target number, and meanwhile, the final optimal sensor configuration is determined.

Step 3. Measure and normalize the dynamic responses $\tilde{\hat{\mathbf{d}}}^{m}$ of the damaged structure, and compute and normalize the dynamic responses $\tilde{\hat{\mathbf{d}}}^{c}(\Delta\alpha^{k})$ of the current FE model at the optimal sensor locations. Correspondingly, the response covariance-based damage index $\mathbf{V}_{pq}^{m}$ and $\mathbf{V}_{pq}^{c}(\Delta\boldsymbol{\alpha}^{k})$ are obtained by using equations (2) and (3), and then substituted into the sensitivity-based damage detection equation (6).

Step 4. Transform equation (6) to a sparse regularized convex optimization problem governed by equation (11). The adaptive regularization factor λ^{*k+1} in equation (11) is calculated by equation (12), in which an estimated solution $\Delta\boldsymbol{\alpha}_{\mathrm{r}}^{k+1}$ for reference can be computed by solving equation (13). Substituting λ^{*k+1} into equation (11), the change of stiffness reduction factor $\Delta\boldsymbol{\alpha}^{k+1}$ is solved by using the convex optimization algorithm SDPT3 which is a predictor-corrector primal-dual path-following approach.

Step 5. Compute the current tolerances $\mathrm{Tol1}(k) = \|\Delta\mathbf{V}_{pq}^{k}\|_2/\|\mathbf{V}_{pq}^{\mathrm{m}}\|_2$ and $\mathrm{Tol2}(k) = \|\Delta\boldsymbol{\alpha}^{k}\|_2/\|\Delta\boldsymbol{\alpha}\|_2$, and calculate the accumulated stiffness reduction factor $\Delta\boldsymbol{\alpha} = \sum\Delta\alpha^{k+1}$

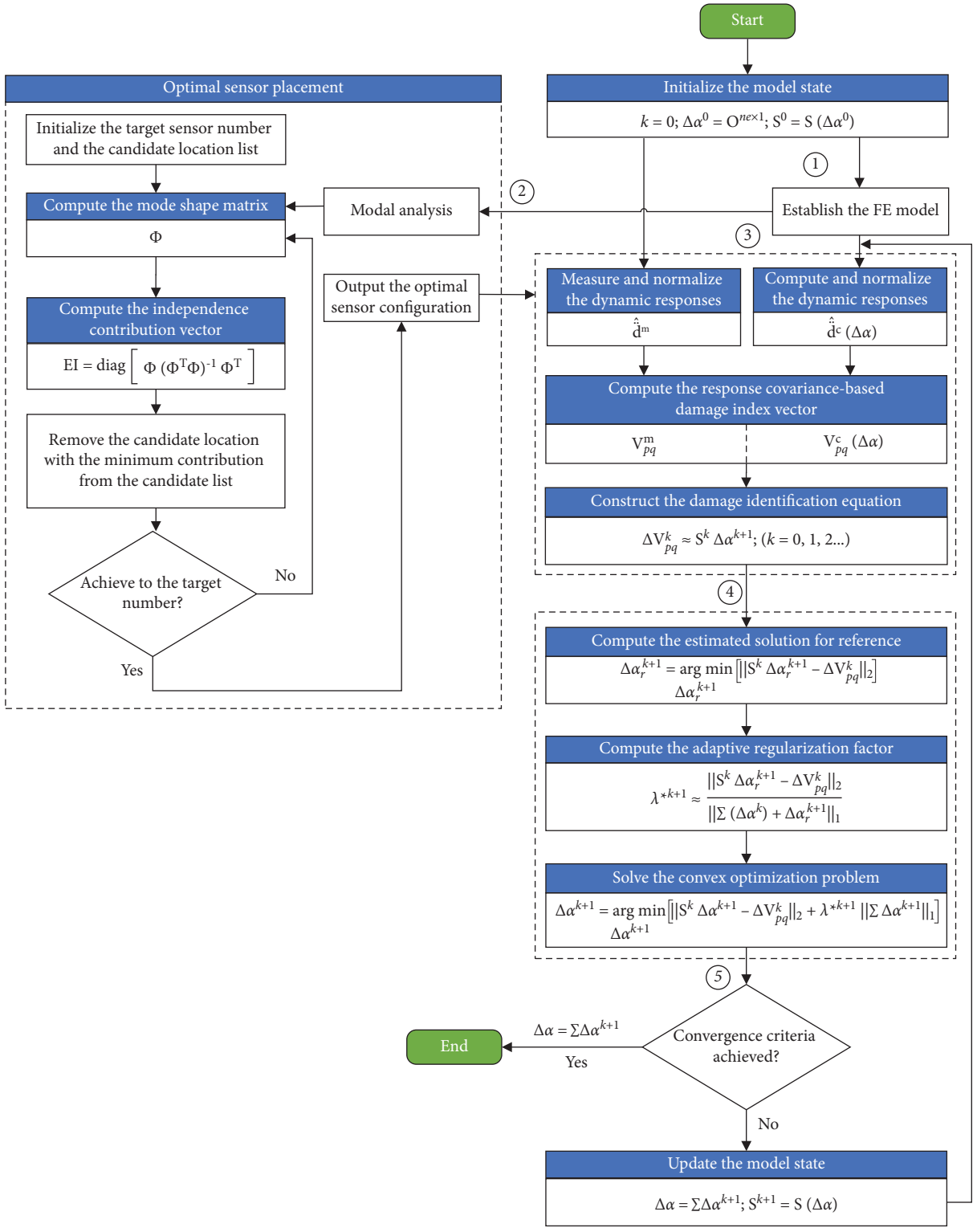

Figure 1: Flowchart of the proposed ASR-based damage detection method.

.$6# If the tolerance-based convergence criteria are not achieved, the FE model and the sensitivity matrix $\mathbf{S}^{k+1} = \mathbf{S}(\Delta\boldsymbol{\alpha})$ are updated with the current $\Delta\boldsymbol{\alpha}$ for the next iteration. Steps 3–5 are conducted iteratively until the convergence criteria are achieved or the preset maximum iteration number is reached. The final accumulated stiffness reduction factor $\Delta\boldsymbol{\alpha}$ is then obtained, in which the damage locations and severities are indicated.

3. Numerical Experiment

3.1. Model Description. An overhanging steel beam shown in Figure 2 is employed to examine the feasibility and accuracy of the proposed adaptive sparse regularization-based damage detection method. The FE model of the beam consists of 41 nodes and 40 equal-length beam elements. The total length of the model is 4 m, and the length, width, and height of each element are 100 mm, 50 mm, and 9.5 mm, respectively. The elastic modulus is 2.05×10^{11} Pa, and the density is 7833kg/m^3. The structural damping is assumed to be Rayleigh damping with the first two damping ratios $\xi_1 = 0.01$ and $\xi_2 = 0.01$, and remains unchanged before and after damage. The beam is subjected to external white noise excitation with a standard deviation of 30N at node 24. For the beam and load given in the numerical experiment, the maximum peak values of stress and strain responses occur in the elements near the supports or in the middle span of the beam. Therefore, elements 12, 20, and 21 are selected as damaged elements in the following study. The sampling ratio in the following study is 200 Hz, which can cover the first 8 modal frequencies, namely 3.06, 5.06, 10.51, 26.01, 39.01, 43.97, 61.15, and 95.65 Hz. Measurement noise can be simulated by a normally distributed random component added to the calculated structural responses [7]. The measured structural response is obtained by the following equation:

$$\ddot{\mathbf{d}}^m = \ddot{\mathbf{d}}^c + N_p \mathbf{N}_{\text{oise}} \text{std}\left(\ddot{\mathbf{d}}^c\right), \tag{14}$$

where $\ddot{\mathbf{d}}^m$ and $\ddot{\mathbf{d}}^c$ with the superscripts m and c represent the noise-polluted acceleration response measured from the damaged structure and the calculated acceleration response of the damaged structure without noise, respectively; N_p is the noise level; $\mathbf{N}_{\text{oise}}$ is a standard normal distribution vector with zero mean and unit standard deviation; $\text{std}(\cdot)$ is the standard deviation operator.

After the FE model is established, the EfI optimal sensor placement is conducted. According to the assumption of EfI, the target mode shape matrix $\mathbf{\Phi}$ should be a rectangle which indicates that the number of sensors is no less than that of the target modes. As illustrated above, the sampling frequency is 200 Hz, and the first 8 modes are covered, and thus the target sensor number is set to be eight. The excitation acts in the vertical direction such that only vertical acceleration responses need to be considered. Nodes 11 and 31 are on the support, so their acceleration responses are equal to zero and there is no need to place accelerometers here. For these reasons, the initial sensor locations include 39 candidates, which are all the nodes except nodes 11 and 31. The EfI contribution vector is computed, and the location with the minimum contribution is removed from the candidate set at each iteration. Finally, the candidate set of sensor locations is iteratively reduced to the target number, and the optimal configuration of sensor locations is shown in Figure 2(a).

3.2. Comparison of Damage Detection Methods under Different Damage Scenarios. A comparison study between the proposed ASR- and the TR-based damage detection methods is conducted by using the overhanging beam model subjected to different noise levels (0%, 5%, and 10%) and different damage scenarios. The approach for adding noise with different levels to the calculated structural responses can refer to equation (14). Three damage scenarios shown in Figure 2 and listed in Table 1 are considered for the subsequent damage detection cases. Specifically, damage scenario 1 (DS1) is the sparsest condition with single damage, i.e., 20% stiffness reduction in E12; damage scenario 2 (DS2) includes two separate defects, i.e., E12 with 20% and E20 with 15% stiffness reduction; and damage scenario 3 (DS3) is a more complicated damage state with the isolated damage in E12 (20% damage) and grouped damages in E20 and E21 (15% and 20% damage).

The two tolerances, Tol1 and Tol2, are used for the updating process in damage detection. Tol1 is the normalized residue of the damage index, which indicates the proximity between the damaged structure and the updated FE model at the current iteration. Tol2 is the normalized accumulated stiffness change at the current iteration, which indicates the stability at the iteration. The maximum iteration number is set to be 200 in this study, and the iteration yielding optimal damage identification result should be chosen after both tolerances converge. The iteration yielding the optimal damage identification result is the one yielding the minimum value of the two tolerance curves.

3.2.1. Damage Scenario with Single Damage. The TR- and ASR-based methods are employed for damage detection in the DS1 scenario. The evolutions of iterative damage identification results by using the two methods are comparatively shown in Figures 3 and 4. In Figure 3, the iterative evolution curves of all 40 elements slowly converge when using the TR-based method; the curve of E12 gradually approaches the red horizontal line standing for 20% stiffness reduction but not reaches the red line, and the two curves of the adjacent elements E11 and E13 have a large deviation from zero. This indicates both the location and severity of the single damage can be identified under different noise levels after 200 iterations, accompanied by obvious false alarms. It is also observed that the identified severity of E12 becomes smaller and the deviations of E11 and E13 become larger with the increase in noise level, indicating that the identification performance gets worse with the increase in noise level. In contrast, it can be seen from Figure 4 with enlarged local graphs that the iterative damage identification evolution curves of all the elements quickly converge when using the ASR-based method, the curve of E12 converges to a stable value very close to the red horizontal line within the first 5 iterations, and meanwhile, the other curves converge to a stable value very close to zero. The comparison between these two cases demonstrates the superiority of the proposed ASR-based method over the TR-based method in the single-damage scenario.

Accordingly, the evolutions of tolerances Tol1 and Tol2 for the two methods are plotted in Figures 5 and 6. After both tolerances converge, the two tolerances are used together to find the iteration step yielding the optimal solution

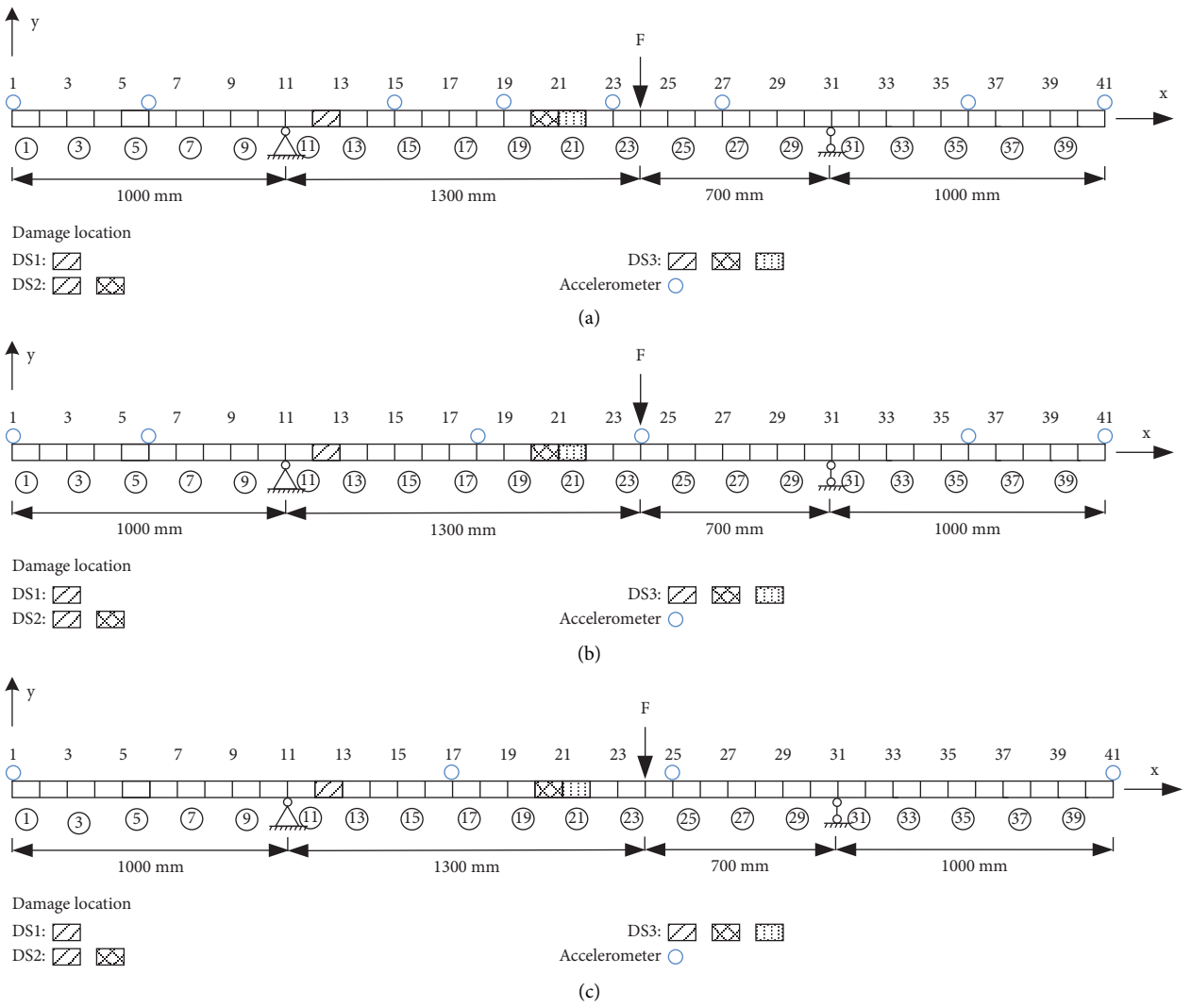

Figure 2: Finite element model of the overhanging beam with damages and the optimal sensor configurations. (a) Optimal sensor configuration of 8 sensors. (b) Optimal sensor configuration of 6 sensors. (c) Optimal sensor configuration of 4 sensors.

Table 1: Description of different damage scenarios for comparison study.

Scenario	Damage element (damage severity)	Noise level	Damage detection method
DS1	E12 (20%)	0%, 5%, 10%	Tikhonov regularization (TR), Adaptive sparse regularization (ASR)
DS2	E12 (20%), E20 (15%)		
DS3	E12 (20%), E20 (15%), E21 (20%)		

marked by red circles in the two figures. In Figure 5, the two tolerance curves for the TR-based method are characterized by a quick decline in the first several iterations and then a very slow decrease till the last iteration step. The minimum tolerance values (red circles in Figure 5) occur at the last iteration step, and they are 5.88×10^{-3}, 1.03×10^{-2}, and 1.54×10^{-2} under the three noise levels. By comparison, it is found from Figure 6 that the two tolerance curves for the ASR-based method are featured by fast convergence to a stable value with small amplitude after a sharp decrease at the first several iterations. Specifically, the minimum tolerance values (red circles in Figure 6) occur at the 14^{th}, 38^{th}, and 12^{th} iteration under the three noise levels, and they are 2.52×10^{-9}, 4.89×10^{-5}, and 3.39×10^{-4}, respectively. The tolerance Tol2 keeps fluctuating with relatively larger amplitudes while Tol1 has slight fluctuation after reaching convergence, which indicates that Tol2 is more sensitive to minor changes at each iteration of model updating.

The damage identification results at the iterations with minimum tolerance values are considered optimal solutions. The optimal solutions for the TR- and ASR-based methods are depicted, respectively, in Figures 7(a) and 7(b) and summarized in Table 2. By using the TR-based method, the identified damage severity of E12 is 18.01%, 16.98%, and

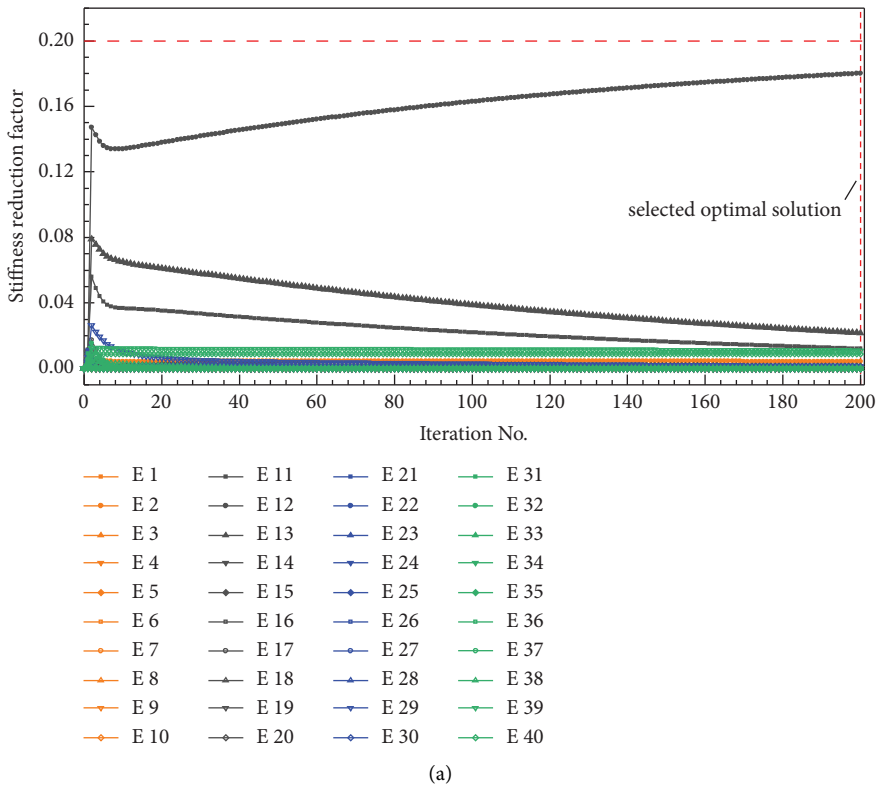

(a)

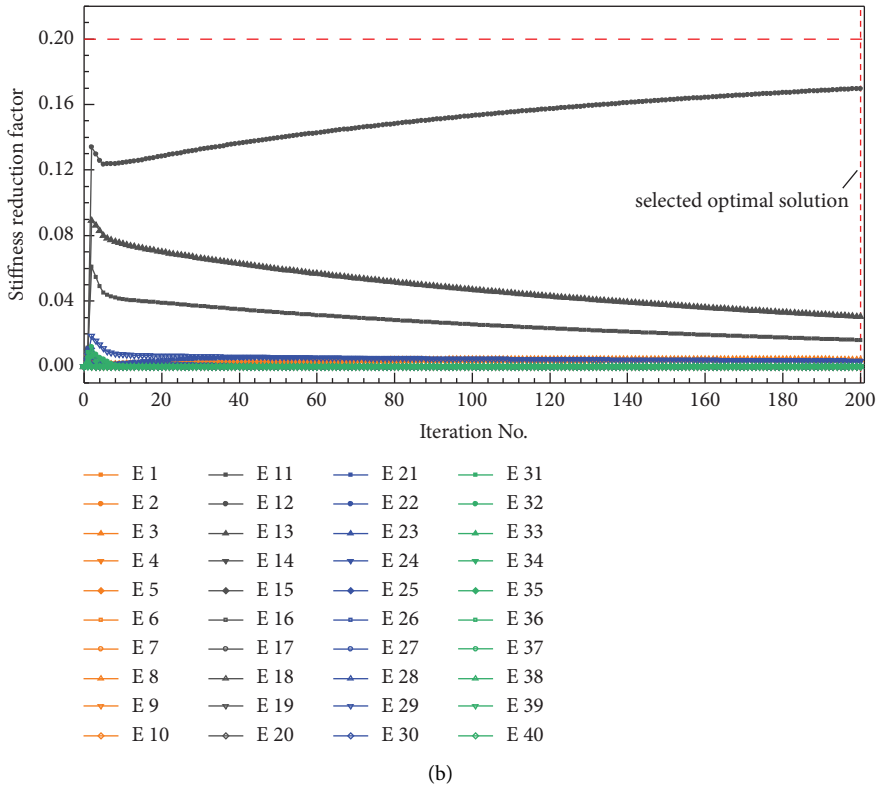

(b)

Figure 3: Continued.

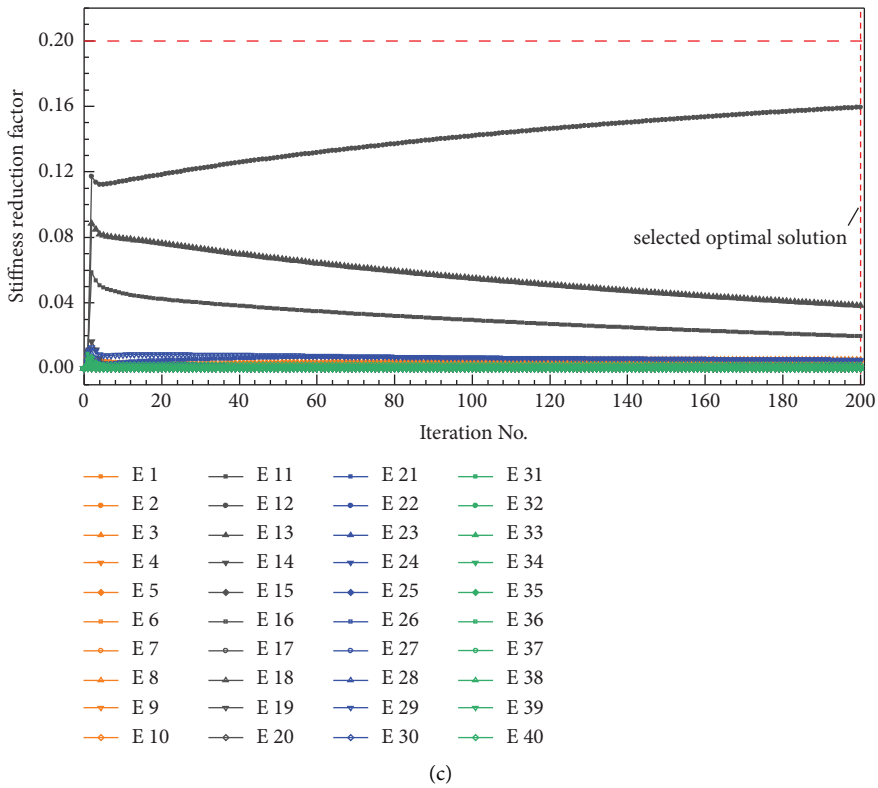

(c)

FIGURE 3: The evolution of iterative damage identification results of DS1 by using the TR-based method. (a) With 0% noise. (b) With 5% noise. (c) With 10% noise.

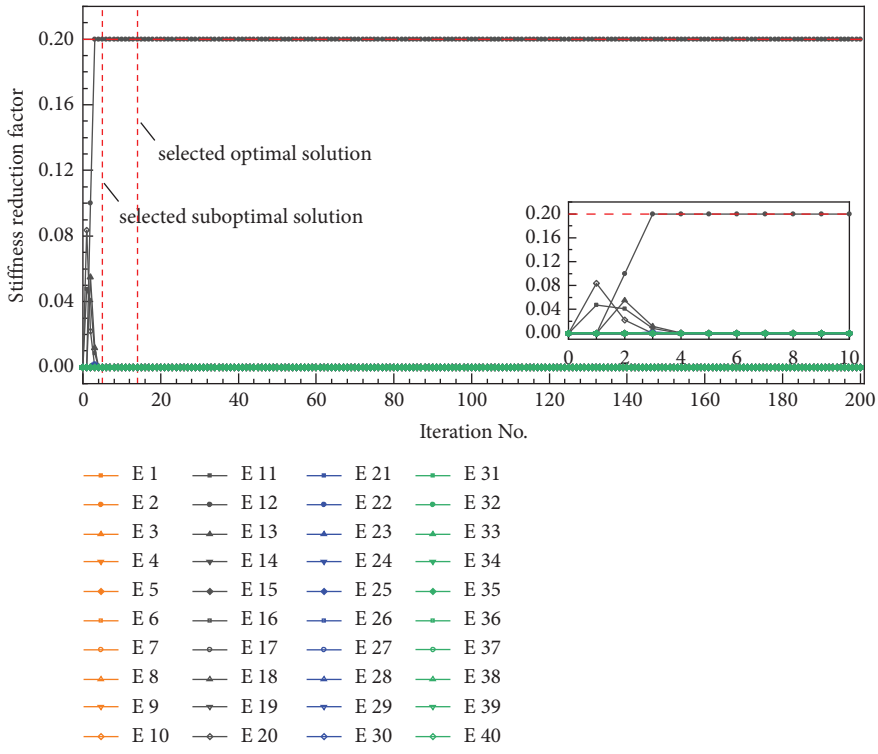

(a)

FIGURE 4: Continued.

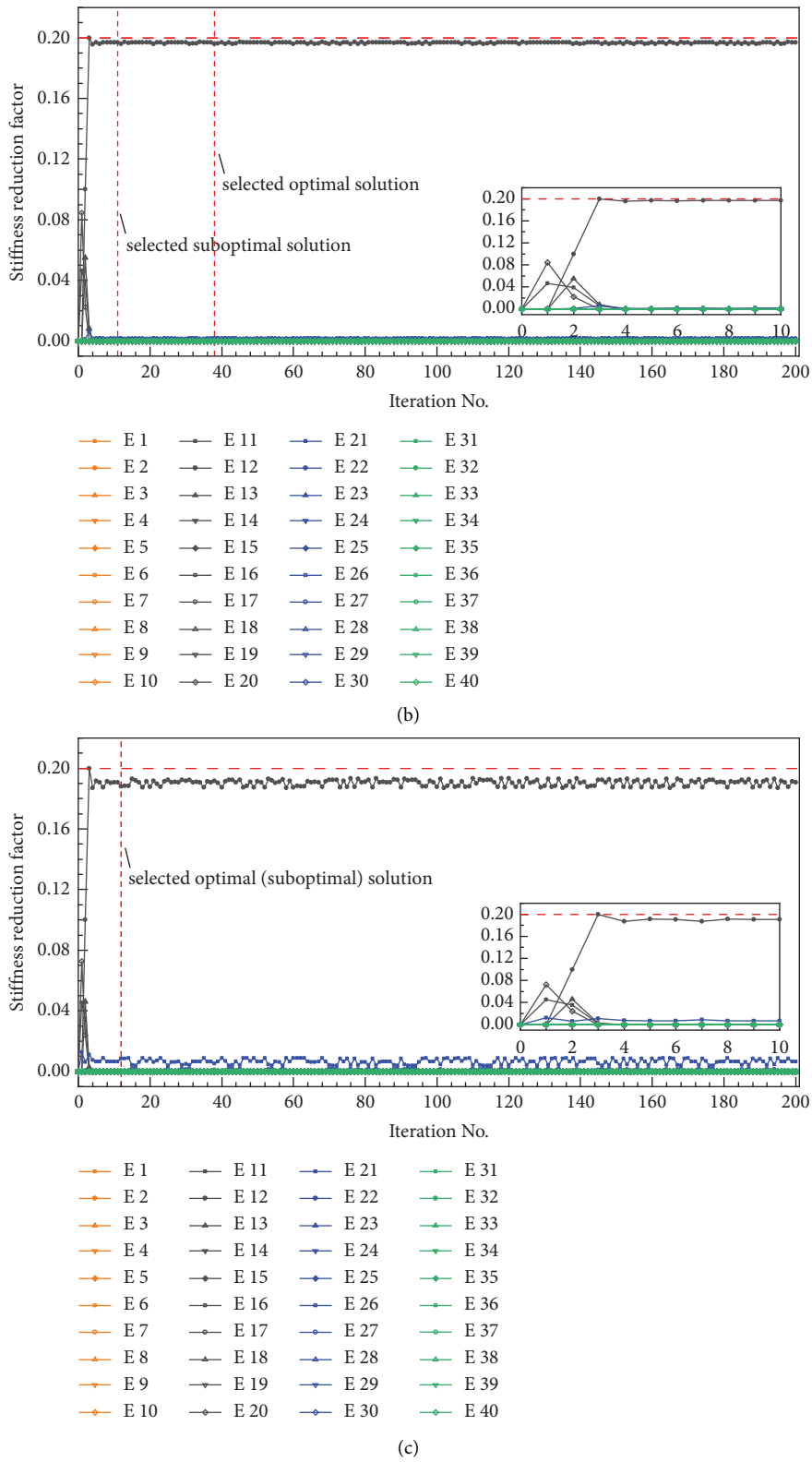

FIGURE 4: The evolution of iterative damage identification results of DS1 by using the ASR-based method. (a) With 0% noise. (b) With 5% noise. (c) With 10% noise.

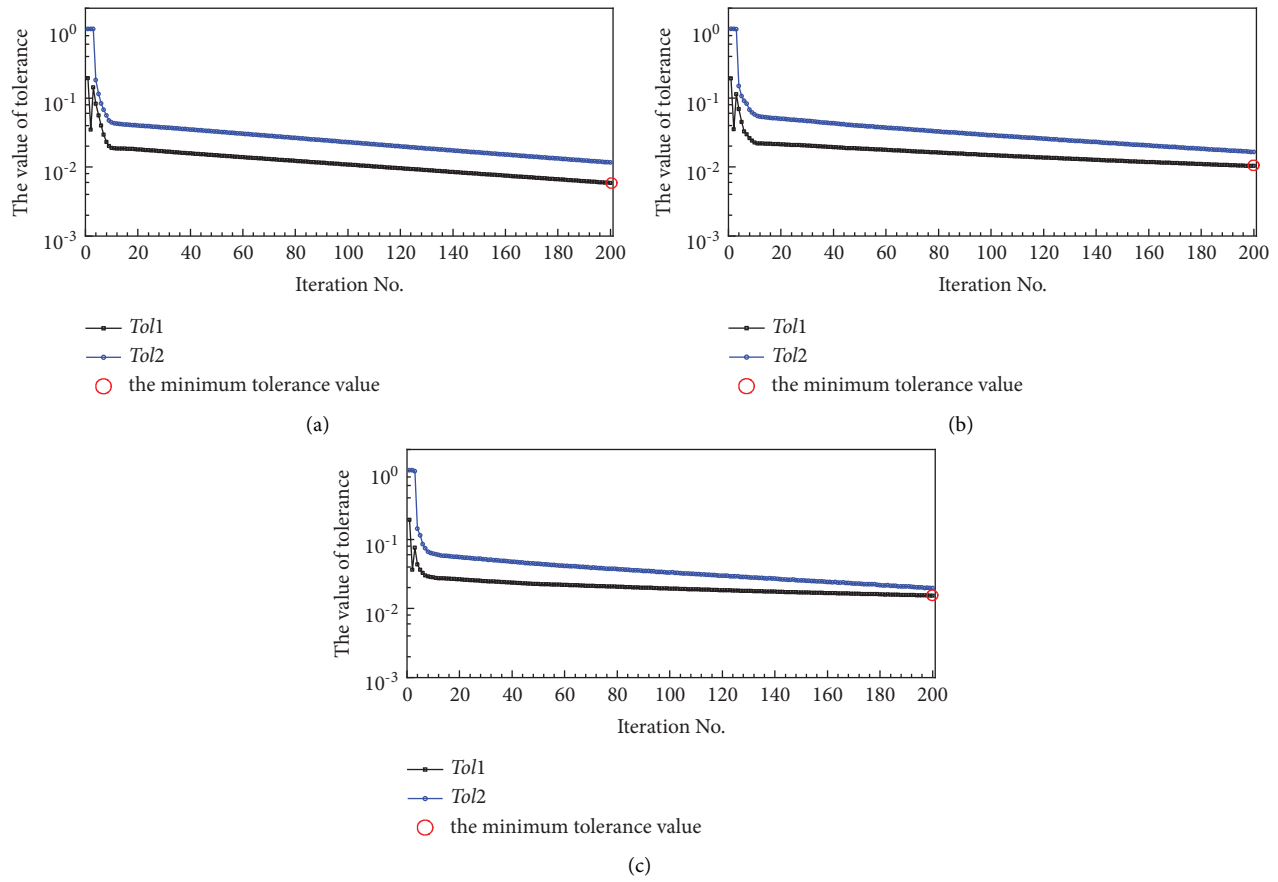

FIGURE 5: The tolerance curves of DS1 by using the TR-based method. (a) With 0% noise. (b) With 5% noise. (c) With 10% noise.

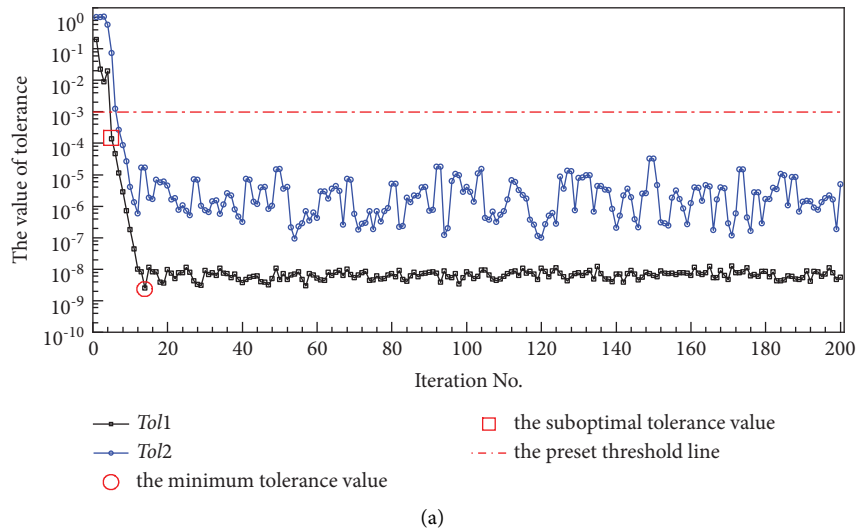

FIGURE 6: Continued.

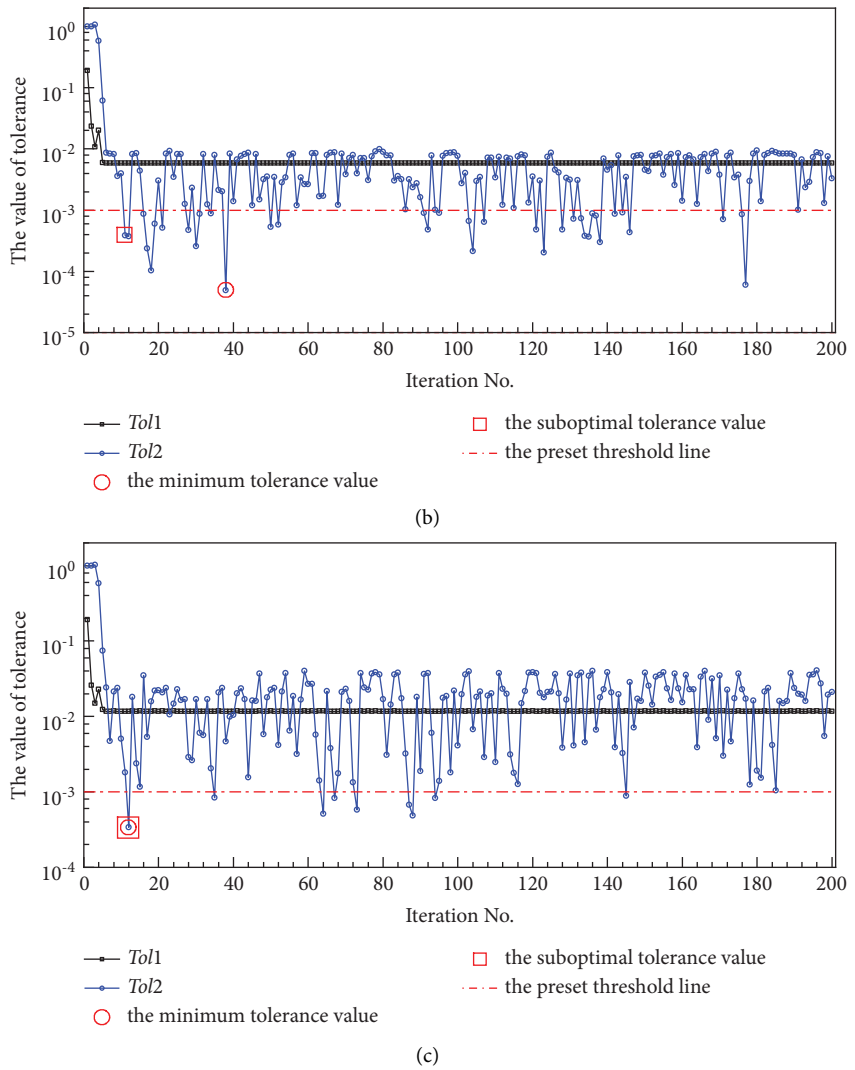

Figure 6: The tolerance curves of DS1 by using the ASR-based method. (a) With 0% noise. (b) With 5% noise. (c) With 10% noise.

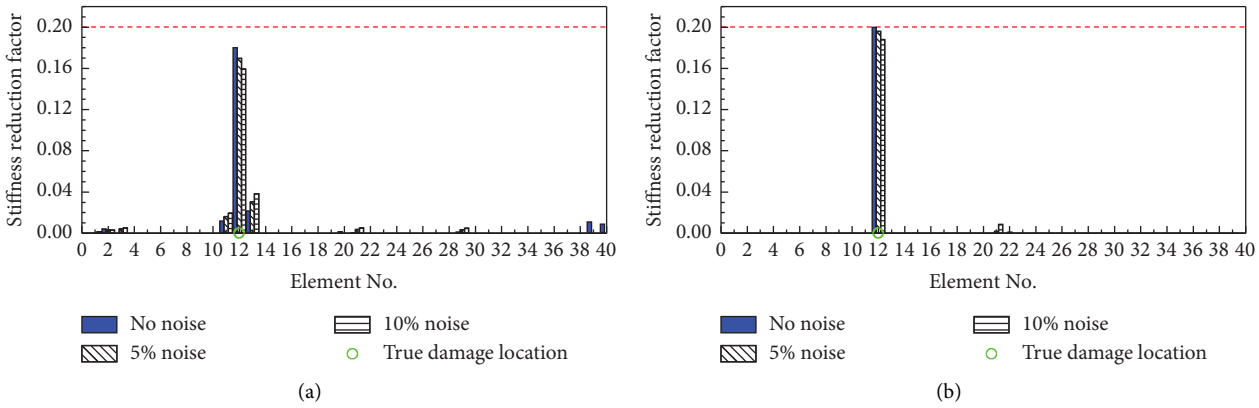

Figure 7: The optimal damage identification solutions of DS1. (a) By using the TR-based method. (b) By using the ASR-based method.

15.95% stiffness reduction, respectively, when subjected to 0%, 5%, and 10% noise levels. The false alarms mainly occur to the adjacent elements E11 and E13, and the maximum false alarms are 2.17%, 3.06%, and 3.84% stiffness reduction in E13 under the different noise levels. By using the ASR-based method, the identified damage severity of E12 is 20%,

Table 2: The identification results of different damage scenarios.

Methods	Noise level (%)	Identified damage (%)			Maximum false alarm (%)		
		DS1	DS2	DS3			
		E12	E12; E20	E12; E20; E21	DS1	DS2	DS3
TR	0	18.01	19.21; 13.37	19.77; 15.17; 19.79	E13 (2.17)	E21 (1.38)	E13 (0.30)
	5	16.98	18.00; 11.74	16.78; 16.32; 18.97	E13 (3.06)	E21 (3.11)	E13 (3.34)
	10	15.95	17.54; 11.05	16.22; 17.04; 18.22	E13 (3.84)	E21 (4.15)	E13 (3.89)
ASR	0	20.00	20.00; 15.00	20.00; 15.00; 20.00	—	—	—
	5	19.60	19.70; 15.07	19.89; 15.94; 19.17	E21 (0.18)	E13 (0.15)	E13 (0.06)
	10	18.80	19.15; 15.36	19.60; 17.08; 18.24	E21 (0.84)	E13 (0.05)	—

19.60%, and 18.80% stiffness reduction, respectively, under the three noise levels. Only one small false alarm happens to E21 with 0.18% and 0.84% stiffness change in the cases of 5% and 10% noise levels. Although both methods can identify the location of the damaged element, the proposed ASR-based method has higher accuracy in damage severity identification. Also, the proposed method has few false alarms with negligible amplitude while the TR-based method has many false alarms with large amplitudes.

The regularization factor plays a significant role to control the balance between the residue norm and solution norm such that both the accuracy and the stability of the iterative damage identification process can be guaranteed. The regularization factor of the TR-based method and the new adaptive regularization factor of the proposed method are, respectively, depicted in Figures 8(a) and 8(b). In Figure 8(a), the regularization factors under the three noise levels decline rapidly from 4.77 at the 1st iteration to 0.67, 0.26, and 0.78 at the 6th iteration and then gradually increase to 0.73, 1.58, and 2.31, respectively. Note that the regularization factors for the TR-based method increase when the noise level becomes higher, which may lead to the over-smoothed solution, the larger residue norm, and data fidelity loss. In contrast, the proposed adaptive regularization factors λ^* of the ASR-based method under the three noise levels witness a drastic decrease at the first little iterations and then converge to stable values with slight fluctuation in amplitude. Specifically, the proposed regularization factors have a sharp reduction from 0.61 at the 1st iteration to a small value close to zero (no noise), a small value with slight fluctuation within 0.06–0.12 (5% noise), and a small value with slight fluctuation within 0.11–0.24 (10% noise). The adaptive regularization factor increases when more noise is added, which can enhance the sparsity of the solution, limit the influence of noise and reduce false alarms. It implies that the automatically determined adaptive regularization factor can effectively adjust the sparsity constraint according to different noise levels such that a better damage detection solution can be obtained.

3.2.2. Damage Scenario with Two Damages. The performance of the ASR-based damage detection method is also examined in the DS2 scenario. The evolution of iterative damage identification results by using the TR- and ASR-based methods are comparatively shown in Figures 9 and 10. As shown in Figure 9, the identification results obtained by using the TR-based method in this scenario are similar to those displayed in Figure 3 for the DS1 scenario. The damage detection process converges slowly, and the results are characterized by correct identification of damage locations, lower severities than the simulated damage levels, and false alarms in the adjacent elements E11, E13, E19, and E21. Comparatively, it is found in Figure 10 that the damage detection process by using the ASR-based method has a fast convergence within the first 5 iterations, and the results are featured by correct identification of damage locations, high accuracy in severity identification, and negligible false alarms under different noise levels. The features of these results are similar to those in Figure 4 for the DS1 scenario. This comparison demonstrates the superiority of the proposed ASR-based method over the TR-based method in the two-damage scenario under the three noise levels.

Accordingly, the evolutions of tolerances Tol1 and Tol2 for the two methods are plotted in Figures 11 and 12. Similar to Figure 5, the curves of the two tolerances obtained by using the TR-based method have a fast decrease at the first several iterations and then a very slow decline till the last iteration step. The minimum tolerance values (red circles in Figure 11) occur at the last iteration step, and they are 6×10^{-3}, 1.17×10^{-2}, and 1.61×10^{-2} under the three noise levels. Differently, it is found from Figure 12 that the two tolerance curves for the ASR-based method are characterized by a sharp decrease at the first several iterations and subsequently fast convergence to a stable value with a small amplitude. The features of these results are similar to those in Figure 6 for the DS1 scenario. Specifically, the minimum tolerance values (red circles in Figure 12) occur at the 124th, 141st, and 179th iteration under the three noise levels, and they are 2.41×10^{-9}, 9.28×10^{-6}, and 2.46×10^{-5}, respectively. Similar to Figure 6, the tolerance Tol2 in this scenario is more sensitive to minor changes than Tol1 at each iteration of model updating, and thus most of the minimum values of tolerance are generated from Tol2.

The damage identification solutions at the iterations with minimum tolerance values are selected as the optimal solutions. The optimal solutions for the TR- and the ASR-based methods are displayed, respectively, in Figures 13(a) and 13(b) and summarized in Table 2. By using the TR-based method, the identified optimal result shown in Figure 13(a) includes the element E12 with 19.21%, 18.00%, and 17.54% stiffness reduction and the element E20 with 13.37%,

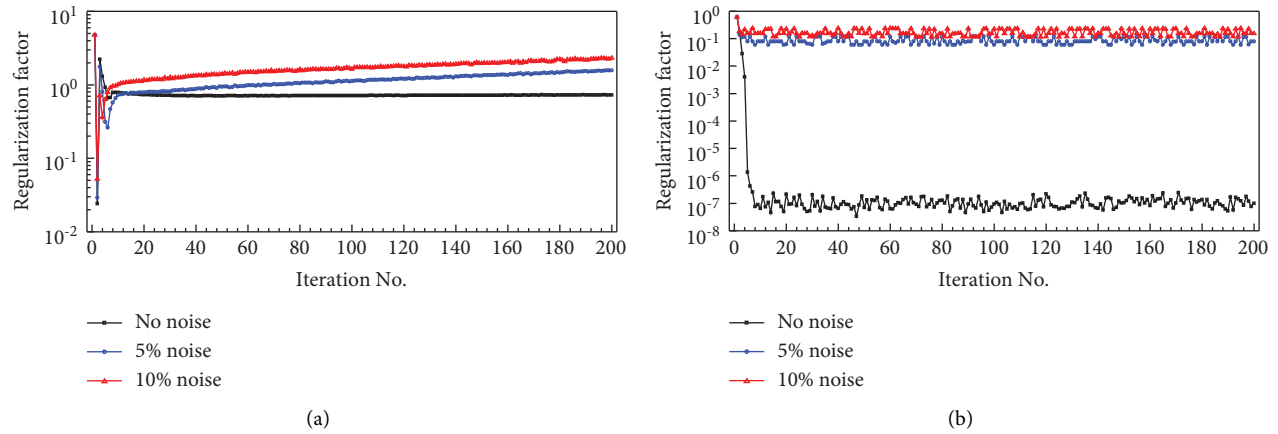

Figure 8: The curves of the regularization factor for DS1. (a) By using the TR-based method. (b) By using the ASR-based method.

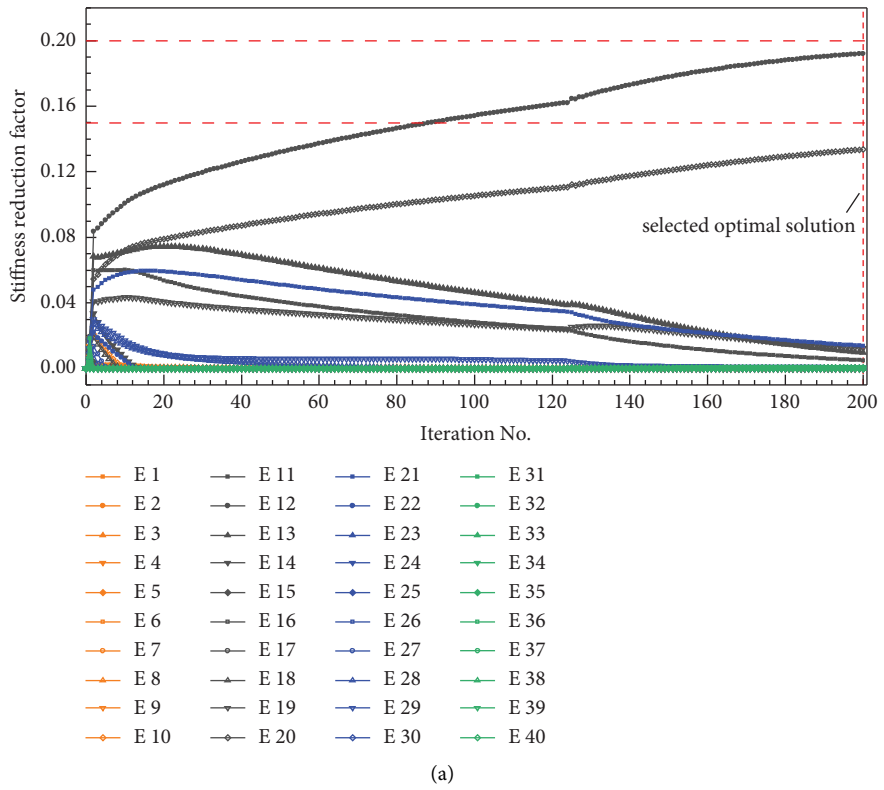

Figure 9: Continued.

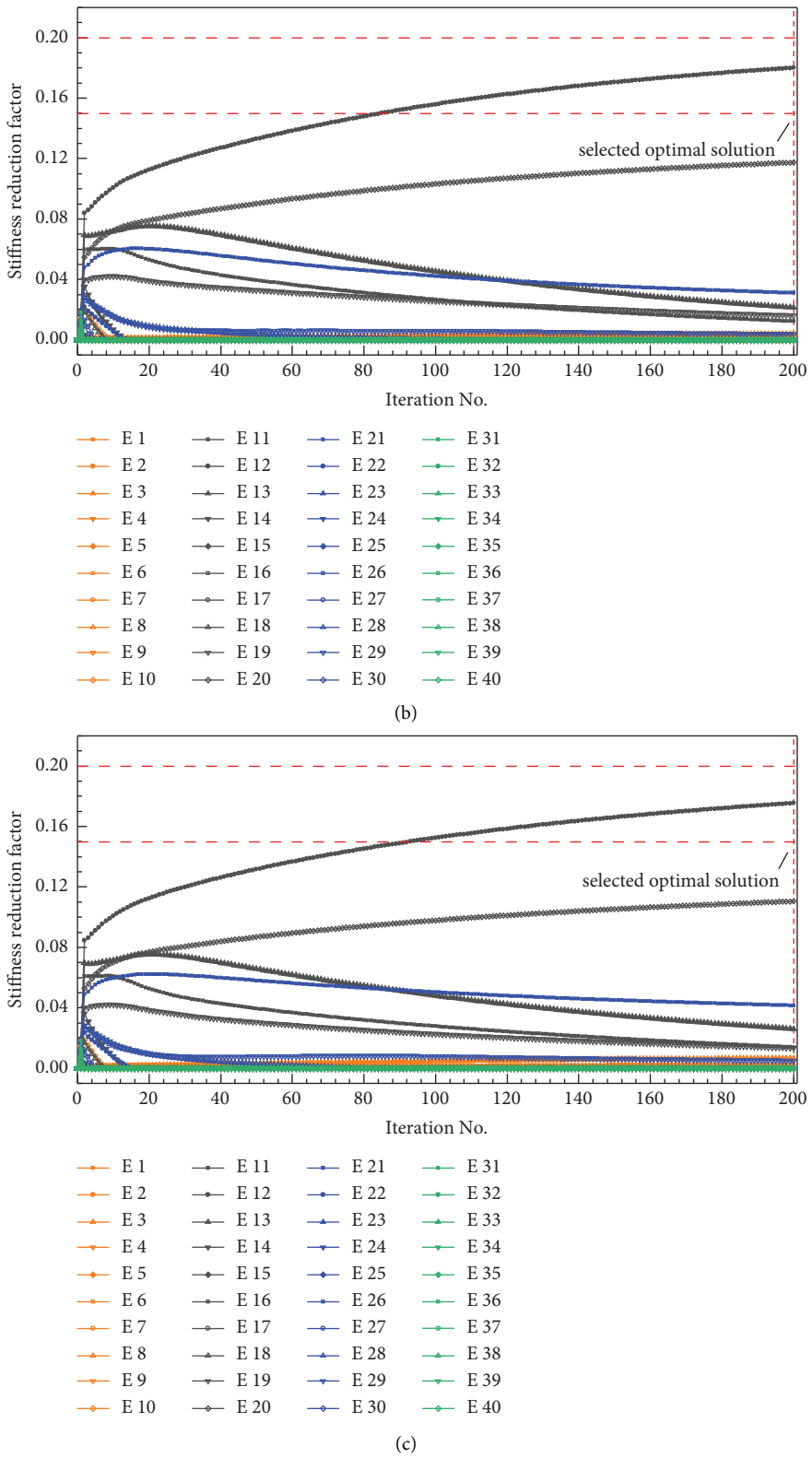

Figure 9: The evolution of iterative damage identification results of DS2 by using the TR-based method. (a) With 0% noise. (b) With 5% noise. (c) With 10% noise.

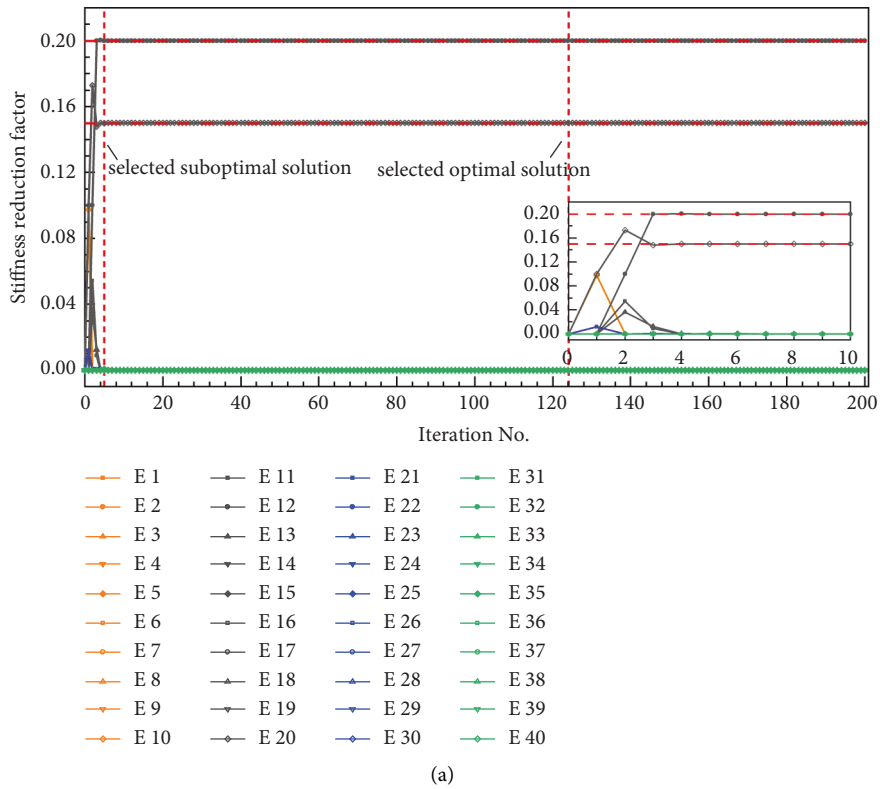

(a)

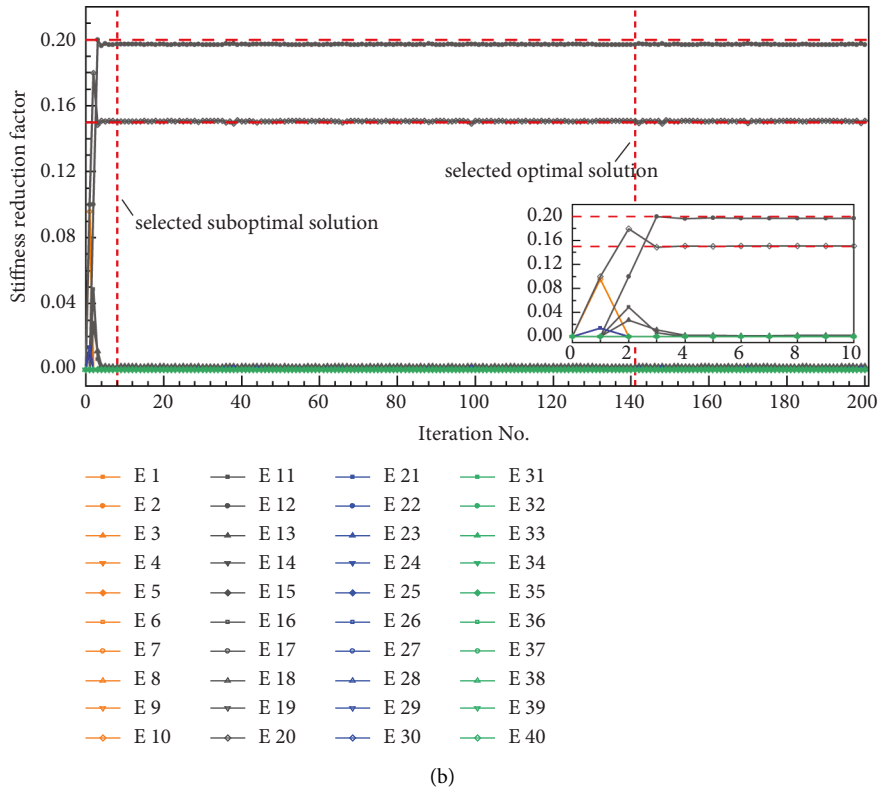

(b)

Figure 10: Continued.

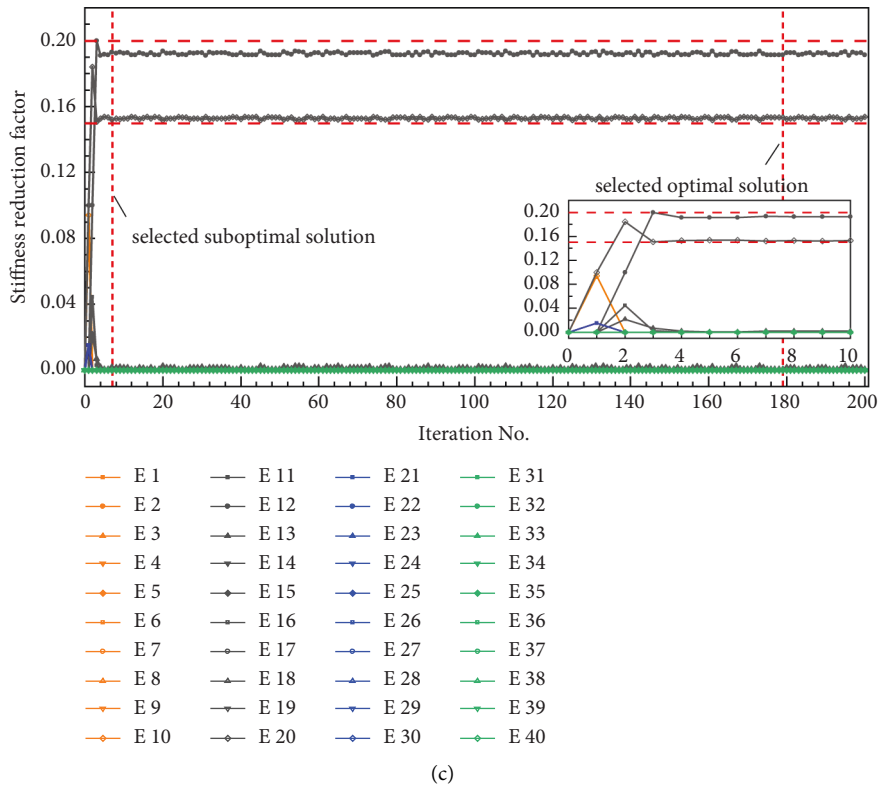

(c)

FIGURE 10: The evolution of iterative damage identification results of DS2 by using the ASR-based method. (a) With 0% noise. (b) With 5% noise. (c) With 10% noise.

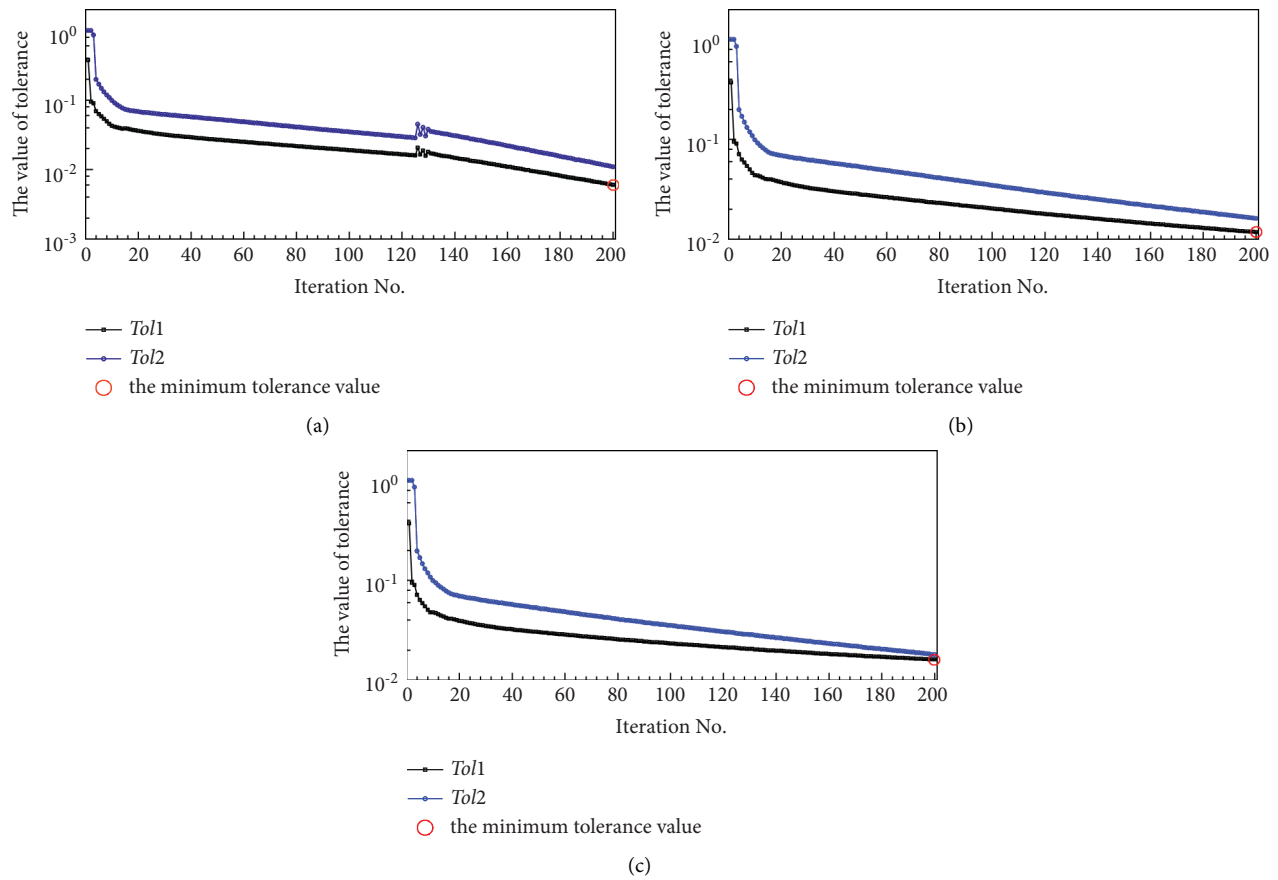

(a) (b)

(c)

FIGURE 11: The tolerance curves of DS2 by using the TR-based method. (a) With 0% noise. (b) With 5% noise. (c) With 10% noise.

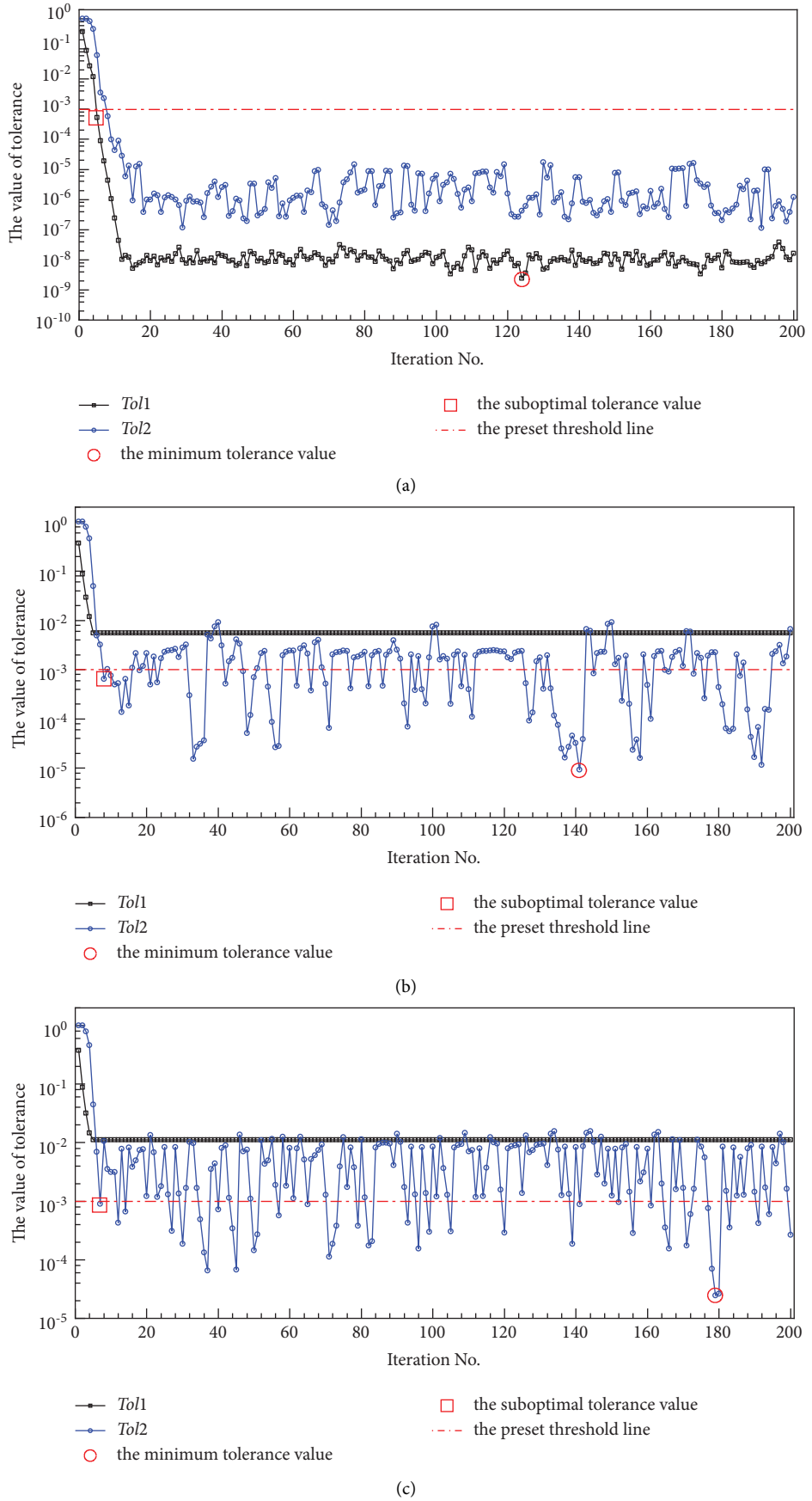

Figure 12: The tolerance curves of DS2 by using the ASR-based method. (a) With 0% noise. (b) With 5% noise. (c) With 10% noise.

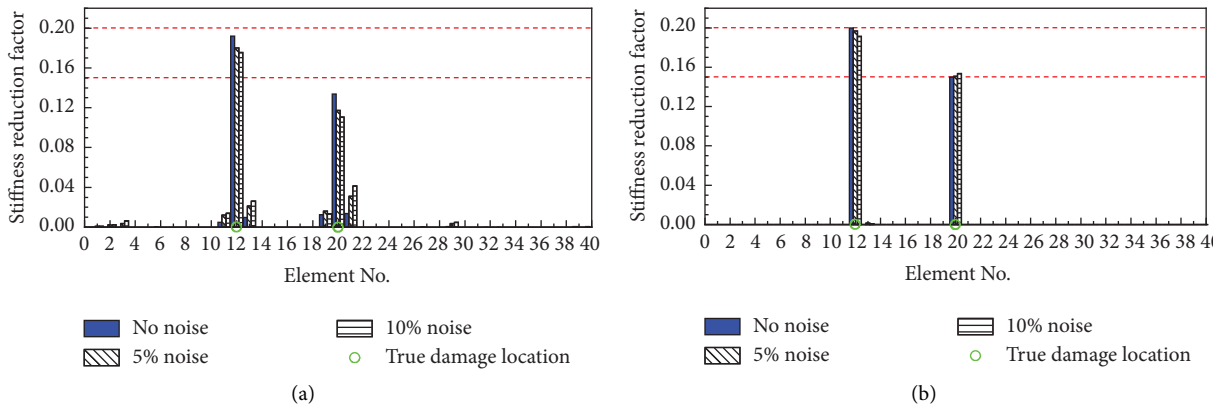

Figure 13: The optimal damage identification solutions of DS2. (a) By using the TR-based method. (b) By using the ASR-based method.

11.74%, and 11.05% stiffness reduction, respectively, when subjected to 0%, 5%, and 10% noise levels. The false alarms mainly occur to the adjacent elements E11, E13, E19, and E21, and the maximum false alarms are 1.38%, 3.11%, and 4.15% stiffness reduction in E21 under the three different noise levels. By using the ASR-based method, the identified result shown in Figure 13(b) includes the element E12 with 20%, 19.70%, and 19.15% damage and the element E20 with 15%, 15.07%, and 15.36% damage, respectively, under the three noise levels. Only one small false alarm happens to E13 with 0.15% and 0.05% stiffness reduction, respectively, in the cases of 5% and 10% noise levels. Both methods can correctly identify the damage locations, but the proposed ASR-based method has higher accuracy in damage severity identification. Also, the proposed method has few false alarms with negligible amplitudes, while the TR-based method has many false alarms with large amplitudes.

In addition, the evolutions of the regularization factors of the ASR-based method are compared with those of the TR-based method in DS2 under different noise levels. The regularization factors of the two methods are illustrated in Figures 14(a) and 14(b), and there is a zoomed picture enlarging the local area within the first 10 iterations in each of the two figures. In Figure 14(a), the regularization factors decrease rapidly from 5.77 at the 1st iteration to 0.85, 0.81, and 0.80 at the 6th iteration under different noise levels, respectively, and then gradually ascend to 0.18, 0.83, and 0.14, respectively. Similar to Figure 8(a) for the DS1 scenario, these values of the regularization factor obtained in this scenario also increase with the increase in noise level. This may result in the over-smoothed solution, the larger residue norm, and data fidelity loss. Comparatively, the proposed regularization factors λ^* of the ASR-based method under the different noise levels are plotted in Figure 14(b). The proposed regularization factors λ^* have a sharp decrease at the first little iterations and then converge to stable values with a slight fluctuation in amplitude. Specifically, the proposed adaptive regularization factors have a sharp reduction from 1.45 at the 1st iteration to a small value close to zero (no noise), a small value with slight fluctuation within 0.04–0.07 (5% noise), and a small value with slight fluctuation within 0.08–0.13 (10% noise). Moreover, it is observed that the initial value of the adaptive regularization factor λ^* is larger than that in DS1, and this can be ascribed to the larger initial residue norm in equation (12). The larger initial residue norm in DS2 is because there are more damages inducing a larger difference between the intact model and the damaged structure than those in DS1. After convergence, the smaller factors λ^* and the bigger solution norms than those in DS1 are obtained, which is coincident with the increased damage in DS2. This implies that the automatically determined adaptive regularization factor can effectively adjust the sparsity constraint according to different damage scenarios, such that a better multidamage detection solution can be obtained.

3.2.3. Damage Scenario with Three Damages. The performance of the ASR-based damage detection method is further examined in the more complex scenario DS3. The evolutions of iterative damage identification result by using the TR- and ASR-based methods are illustrated in Figures 15 and 16. As shown in Figure 15, the identification results obtained by using the TR-based method in this scenario are similar to those displayed in Figures 3 and 9 in scenarios DS1 and DS2. The damage detection process converges slowly, and the results are characterized by correct identification of damage locations, lower severities than the simulated damage levels, and false alarms in the adjacent elements E11 and E13. In contrast, the damage detection process by using the ASR-based method has a fast convergence within the first 8 iterations, and the results are featured by correct identification of damage locations, high accuracy in severity identification, and negligible false alarms under different noise levels. The features of these results are similar to those in Figures 4 and 10 in DS1 and DS2. Though the performance of the ASR-based method in this scenario is not as good as that in DS1 and DS2, it still keeps obvious advantages over the TR-based method in accuracy and convergence speed.

Accordingly, the evolutions of tolerances Tol1 and Tol2 for the two methods are illustrated in Figures 17 and 18. Similar to Figures 5 and 11, the curves of the two tolerances obtained by using the TR-based method experience a fast decrease at the first several iterations and then a very slow

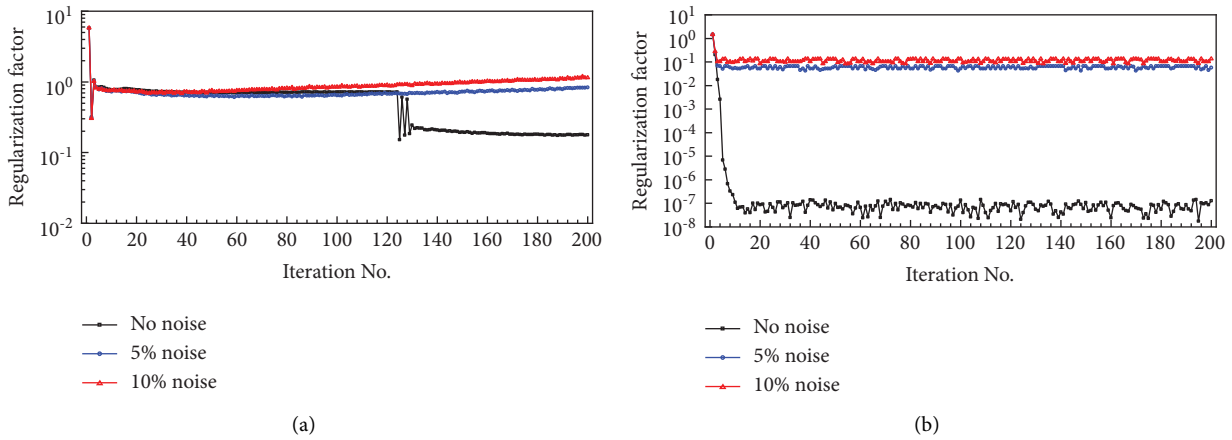

FIGURE 14: The curves of the regularization factor for DS2. (a) By using the TR-based method. (b) By using the ASR-based method.

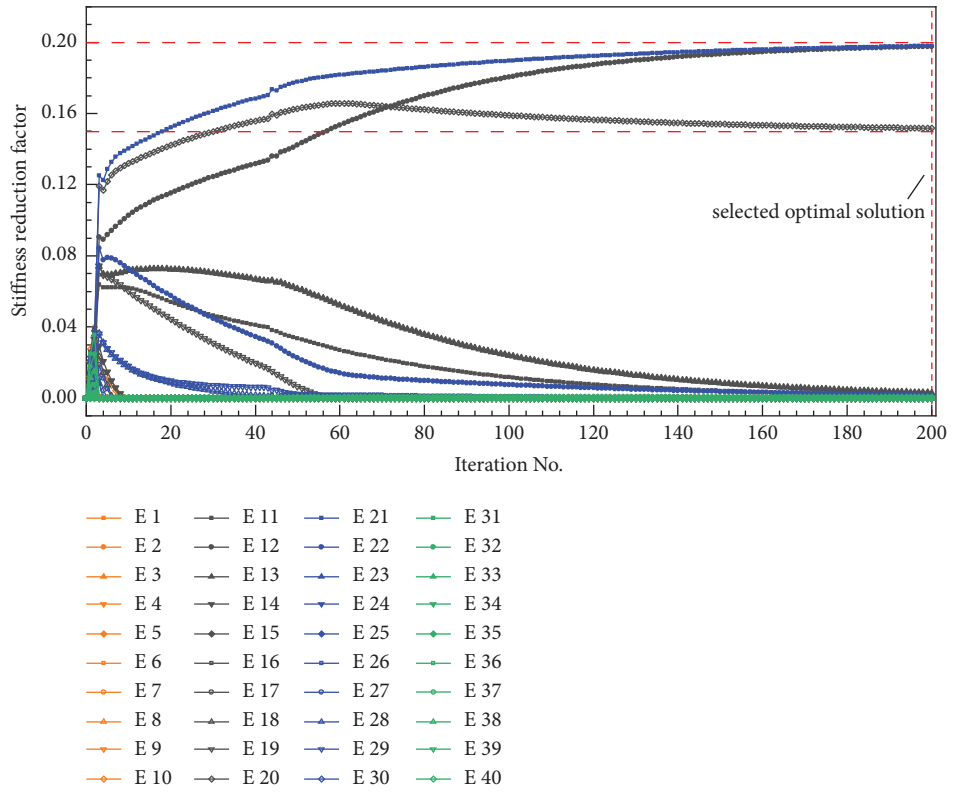

FIGURE 15: Continued.

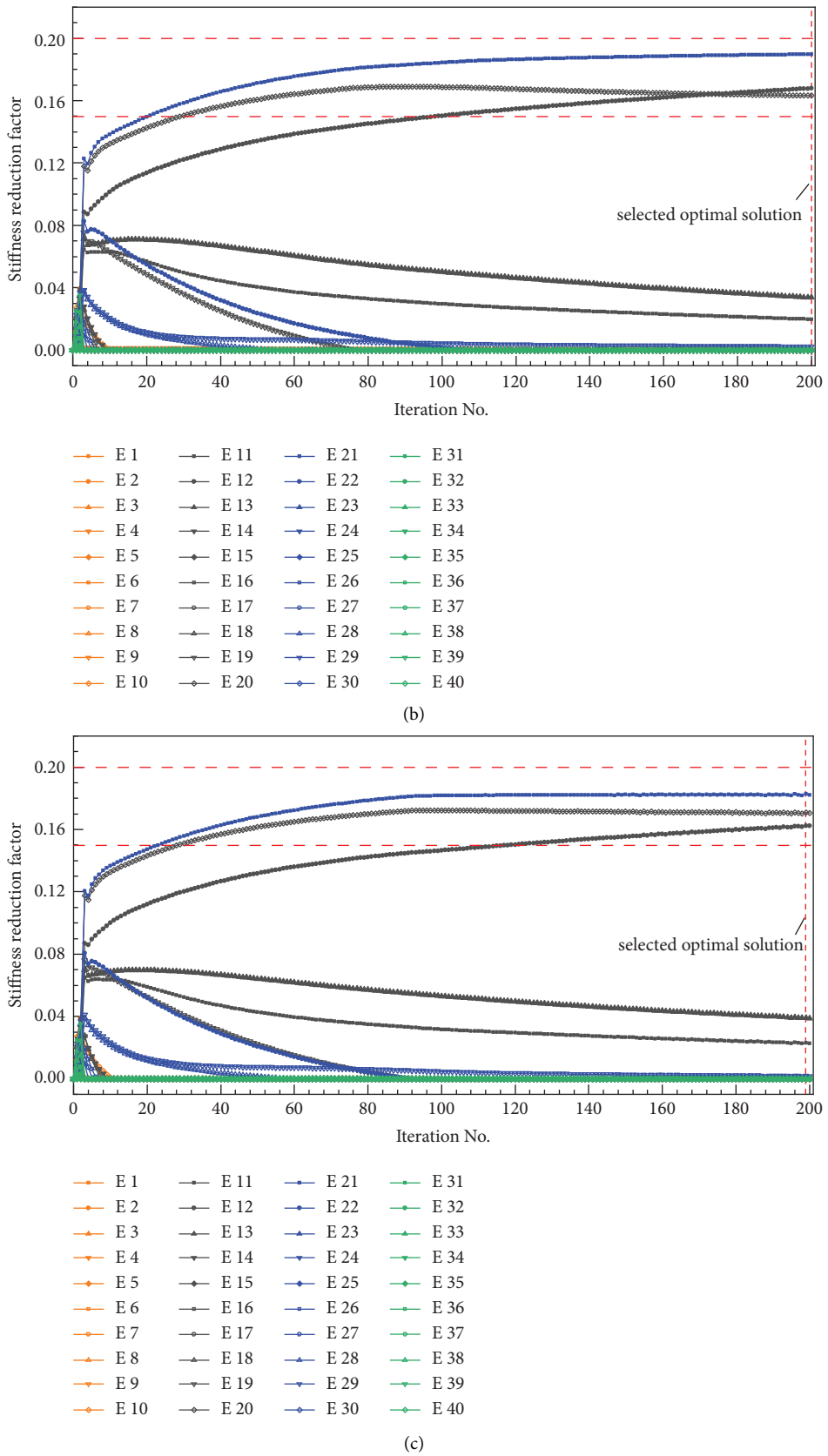

FIGURE 15: The evolution of iterative damage identification results of DS3 by using the TR-based method. (a) With 0% noise. (b) With 5% noise. (c) With 10% noise.

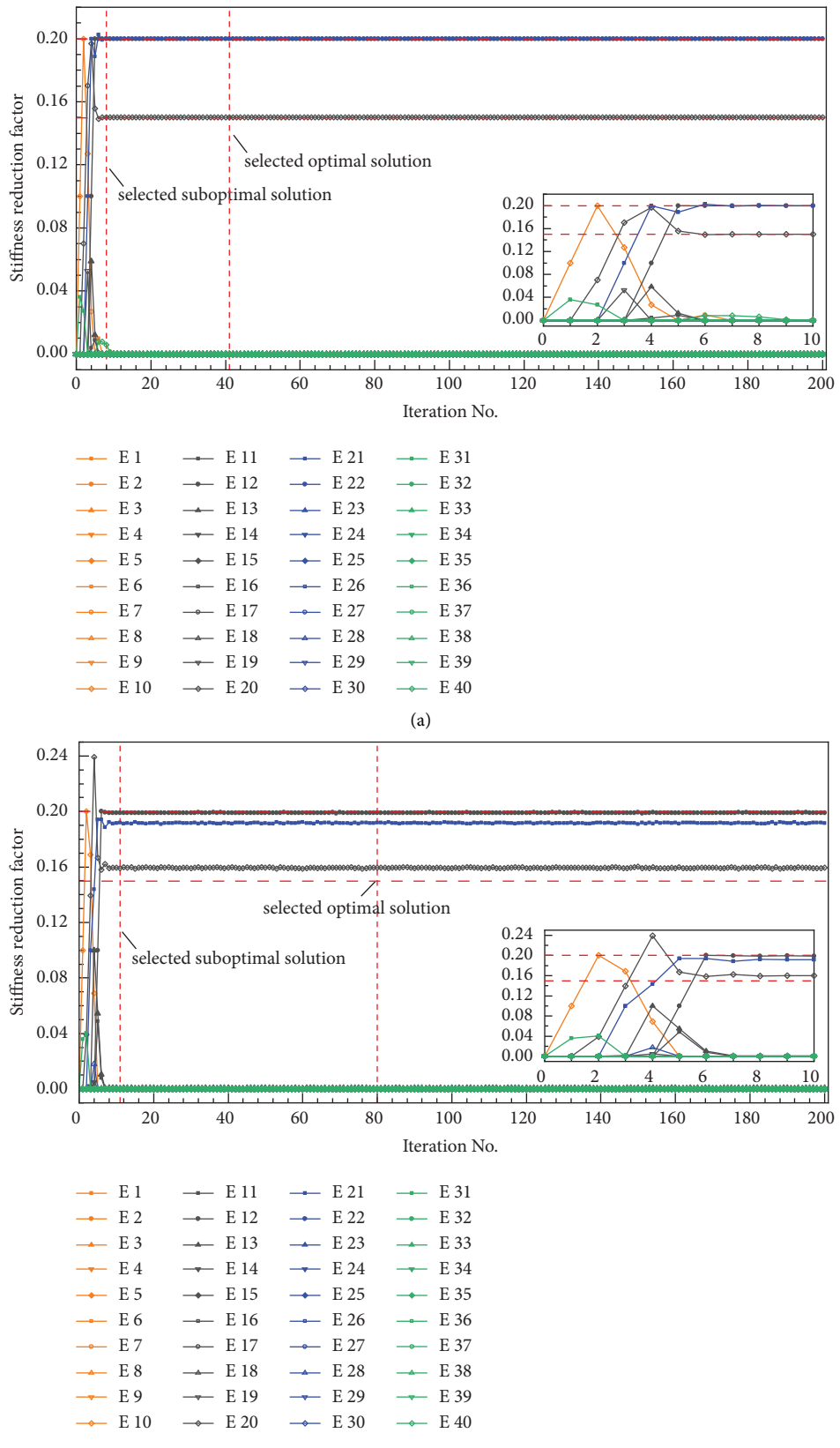

(a)

(b)

Figure 16: Continued.

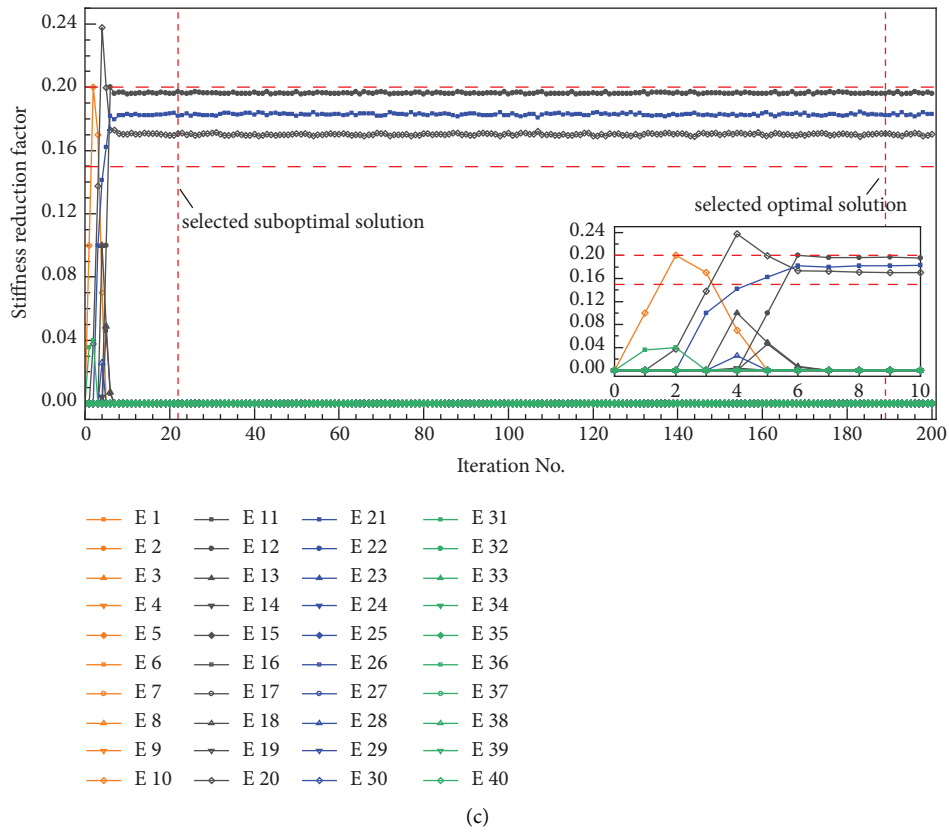

(c)

FIGURE 16: The evolution of iterative damage identification results of DS3 by using the ASR-based method. (a) With 0% noise. (b) With 5% noise. (c) With 10% noise.

decline till the last iteration step. The minimum tolerance values (red circles in Figure 17) occur at the last iteration step, and they are 1.34×10^{-3}, 1.05×10^{-2}, and 7.45×10^{-3} under the three noise levels. Differently, it is found from Figure 18 that the two tolerance curves for the ASR-based method are featured by a sharp decrease at the first several iterations and then fast convergence to a stable value with a small amplitude. The features of these results are similar to those in Figures 6 and 12 in DS1 and DS2. Specifically, the minimum tolerance values (red circles in Figure 18) occur at the 41^{st}, 80^{th}, and 189^{th} iteration under the three noise levels, and they are 3.07×10^{-9}, 7.99×10^{-5}, and 1.85×10^{-4}, respectively. Similar to Figures 6 and 12, the tolerance Tol2 in this scenario is more sensitive to minor changes than Tol1 at each iteration, and thus most of the minimum values of tolerance are found from Tol2.

The damage identification solutions at the iterations with minimum tolerance values are chosen as the optimal solutions. The optimal solutions obtained by the TR- and the ASR-based methods are displayed, respectively, in Figures 19(a) and 19(b) and summarized in Table 2. By using the TR-based method, the identified optimal result shown in Figure 19(a) includes the element E12 with 19.77%, 16.78%, and 16.22% stiffness reduction, the element E20 with 15.17%, 16.32%, and 17.04% stiffness reduction, and the element E21 with 19.79%, 18.97%, and 18.22% stiffness reduction, respectively, when subjected to 0%, 5%, and 10% noise levels. The false alarms mainly occur to the adjacent elements E11 and E13, and the maximum false alarms are 0.30%, 3.34%, and 3.89% stiffness reduction in E13 under the different levels of noise. By using the ASR-based method, the identified result shown in Figure 19(b) includes the element E12 with 20%, 19.89%, and 19.60% damage, the element E20 with 15%, 15.94%, and 17.08% damage, and the element E21 with 20%, 19.17%, and 18.24% damage under different levels of noise, respectively. Only one negligible false alarm occurs in E13 with 0.06% stiffness reduction under 5% noise. Note that both two methods can correctly identify the damage locations, but the proposed method can provide higher accuracy in damage severity identification and few false alarms with negligible amplitudes.

Further, the evolutions of the regularization factors of the ASR-based method are compared with those of the TR-based method under different noise levels in DS3. The regularization factors of the two methods are illustrated in Figures 20(a) and 20(b), and there is a zoomed picture enlarging the local area within the first 10 iterations in each of the two figures. In Figure 20(a), the regularization factors decrease rapidly from 6.91 at the 1^{st} iteration to 0.83, 0.92, and 1.00 at the 6^{th} iteration under different noise levels, and then gradually increase to 0.14, 1.41, and 3.80, respectively. Similar to Figures 8(a) and 14(a) for the scenarios DS1 and DS2, these values of the regularization factor obtained in this scenario also ascend with the increase in noise level. This

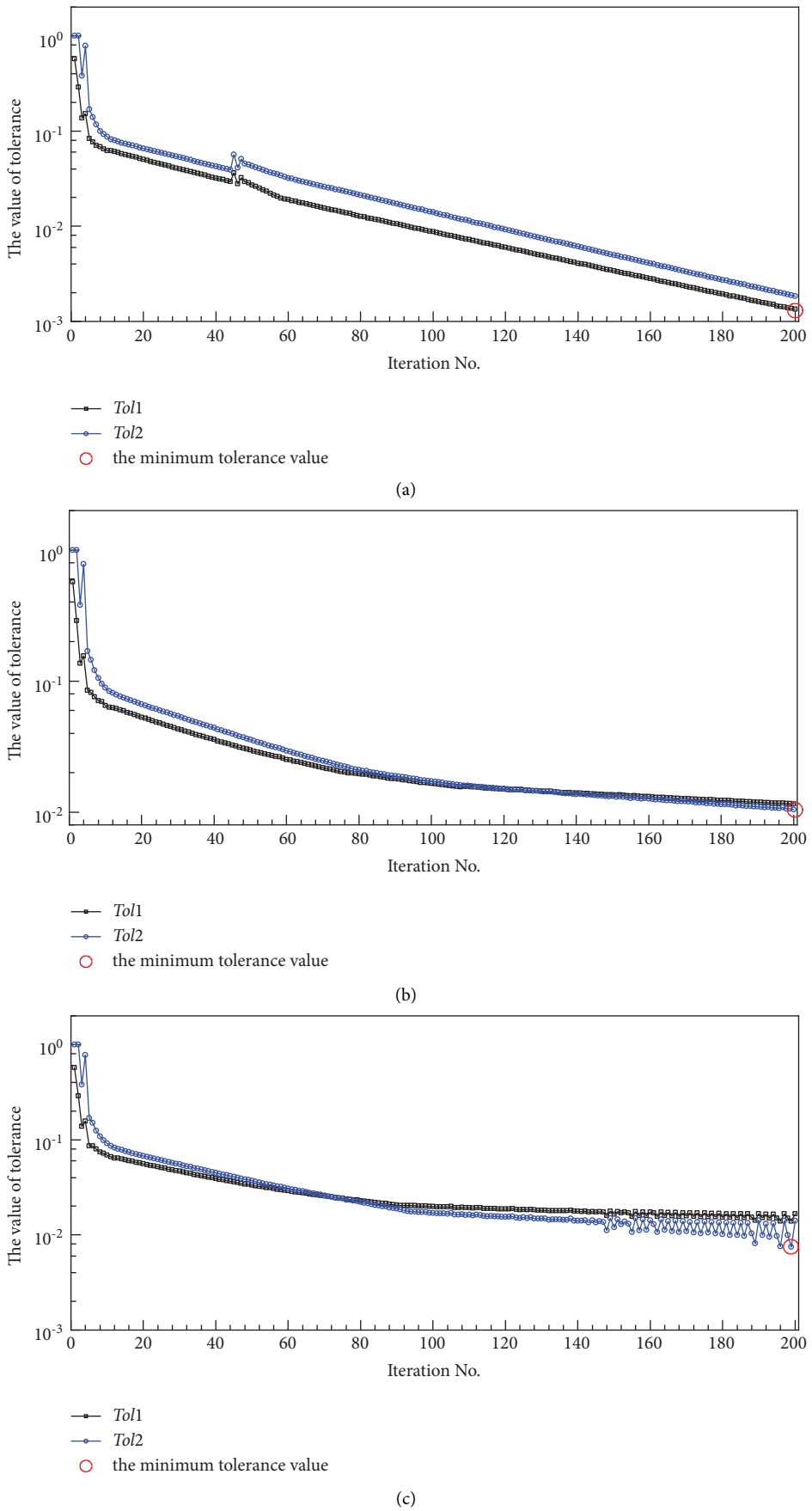

Figure 17: The tolerance curves of DS3 by using the TR-based method. (a) With 0% noise. (b) With 5% noise. (c) With 10% noise.

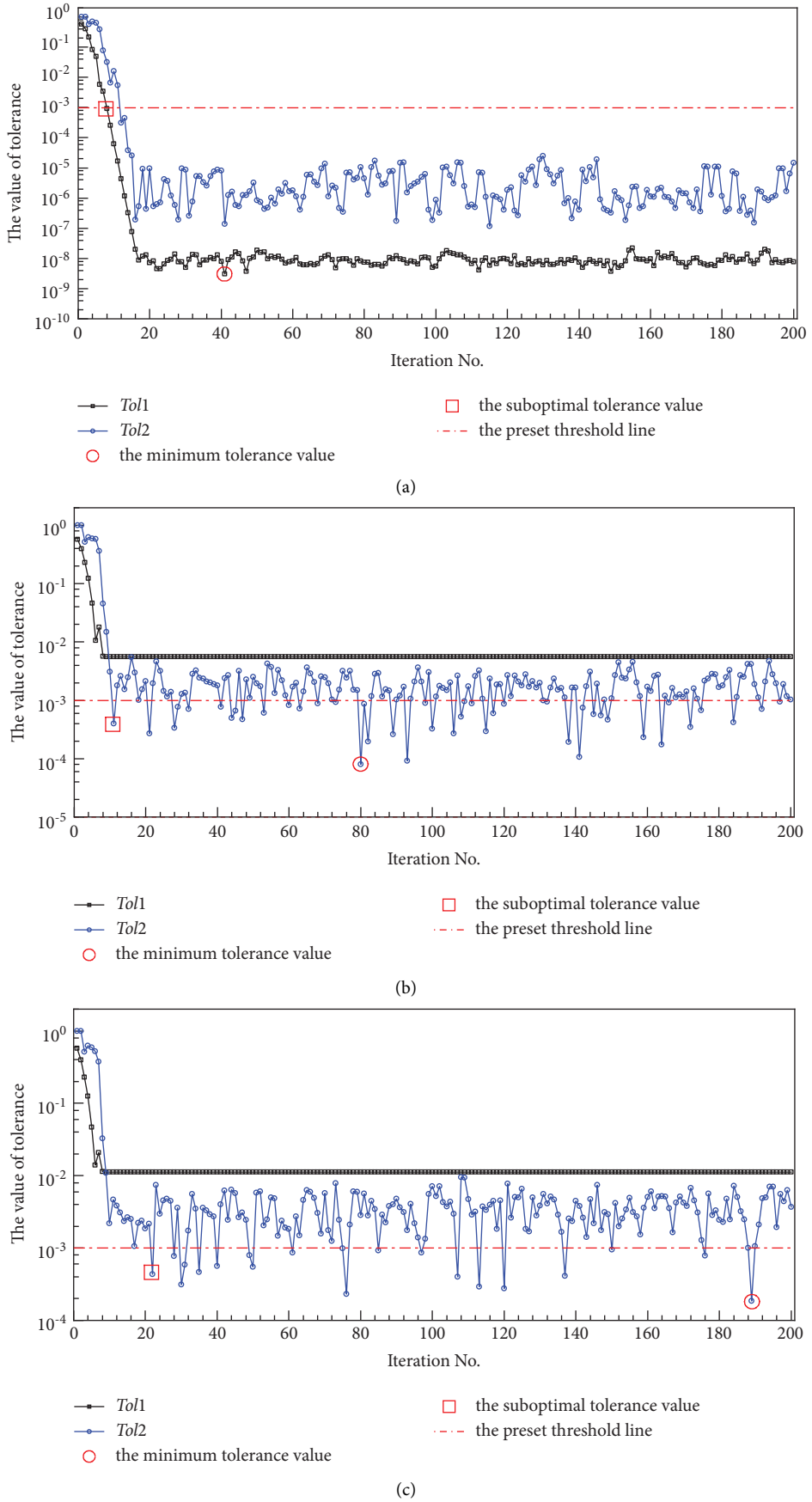

Figure 18: The tolerance curves of DS3 by using the ASR-based method. (a) With 0% noise. (b) With 5% noise. (c) With 10% noise.

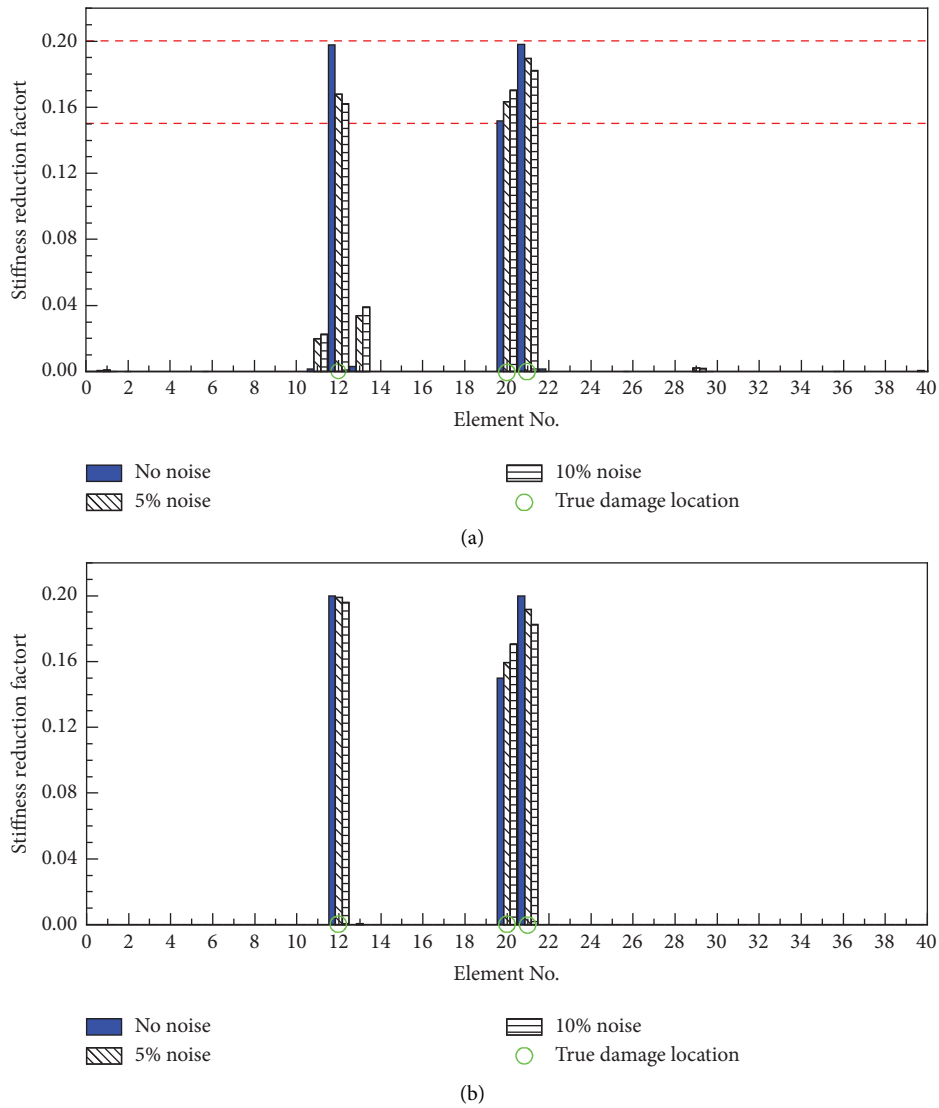

Figure 19: The optimal damage identification solutions of DS3. (a) By using the TR-based method. (b) By using the ASR-based method.

may lead to the oversmoothed solution, the larger residue norm, and data fidelity loss. Comparatively, the proposed regularization factors λ^* of the ASR-based method under the different noise levels are illustrated in Figure 20(b). The proposed regularization factors λ^* have a sharp decrease at the first little iterations and then converge to stable values with slight fluctuation in amplitude. Specifically, the proposed adaptive regularization factors have a sharp reduction from 3.33 at the 1st iteration to a small value close to zero (no noise), a small value with slight fluctuation within 0.03–0.06 (5% noise), and a small value with slight fluctuation within 0.06–0.11 (10% noise). Moreover, the initial value of the adaptive regularization factor λ^* is larger than those in DS2 and DS1, and this can be ascribed to the situation that there are more damages inducing a larger difference between the intact model and the damaged structure in DS3. After convergence, the method has smaller factors λ^* and bigger solution norms than those in DS1 and DS2, which is consistent with the increased damage in DS3. This implies that the automatically determined adaptive regularization factor can effectively adjust the sparsity constraint for achieving better multidamage detection performance in the complex multidamage scenario.

4. Discussions

4.1. Comparison of Time Consumption and Identification Accuracy by Using Two Strategies. The time consumption of the TR- and ASR-based damage detection methods are compared in different damage scenarios with various noise levels and listed in Table 3. The common basis for comparison is that a workstation with the same hardware specifications is used in all cases, and the hardware is the DELL Precision 7920 Tower workstation with the Intel(R) Xeon(R) Gold 6248R CPU @ 3.00 GHz × 2 and 512G RAM. There are nine cases in total due to the combination of three damage scenarios and three noise levels in each damage scenario. The time consumption for solving the damage

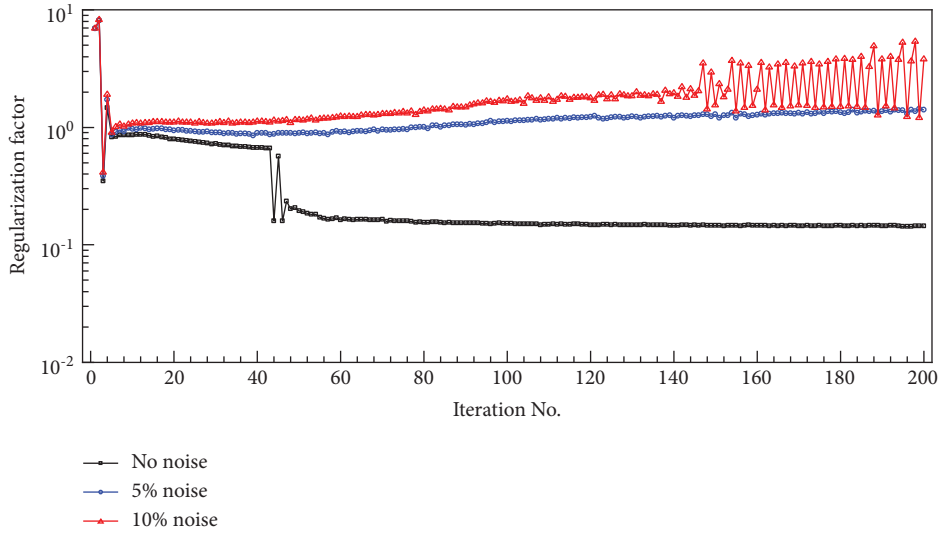

(a)

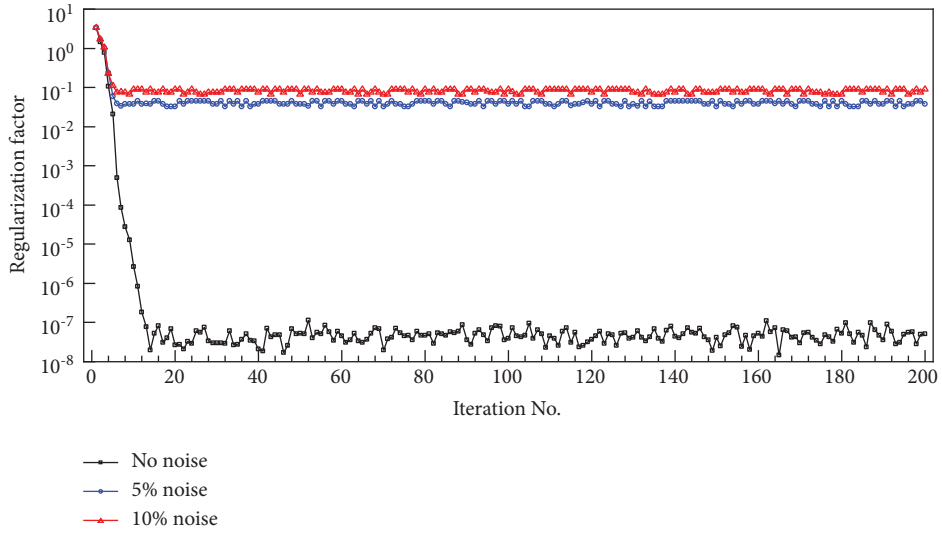

(b)

Figure 20: The curves of the regularization factor for DS3. (a) By using the TR-based method. (b) By using the ASR-based method.

Table 3: Time consumption of damage identification by using the TR- and ASR-based methods.

Selection strategy	Scenario	Method	Time consumption		
			0% noise (s)	5% noise (s)	10% noise (s)
Strategy 1	DS1	TR	1160	1149	1167
		ASR	2318	2380	2357
	DS2	TR	1046	1043	1042
		ASR	2343	2397	2376
	DS3	TR	1034	1052	1067
		ASR	2308	2357	2323
Strategy 2	DS1	ASR	66	58	92
	DS2		130	93	126
	DS3		139	81	260

detection problem and obtaining an optimal solution is related to strategies used to determine the optimal one. There are two strategies in this study. In Strategy 1, an optimal solution is determined by using the minimum value of both tolerances after completing the preset number of iterations. The preset number of iterations is 200 in this

study, which is sufficient for the iterative updating processes to converge. In Strategy 2, an optimal solution is considered as the first solution, which guarantees that the tolerance of this solution is lower than a preset small threshold. It is the suboptimal solution for terminating the search process when identification accuracy becomes acceptable. The threshold value is set to be 10^{-3}. Specifically, the maximum durations of computation time for the TR-based method to complete the 200 iteration steps are, respectively, 1167s, 1046s, and 1067s under the three damage scenarios. Comparatively, the maximum time consumption for the ASR-based method to complete the same number of iterations are, respectively, 2380s, 2397s, and 2357s under the same damage scenarios. In each case, the minimum value of both tolerances is then found among the 200 iterations for determining the iteration yielding the optimal solution. The minimum tolerance values when applying Strategy 1 in Sections 3.2.1–3.2.3 are represented by the red circles in Figures 5, 6, 11, 12, 17, and 18. Note that the computation time of the ASR-based method is about twice that of the TR-based method when the two methods complete the same number of iterations. The reason is that the ASR-based method does not have a closed-form solution such as the TR-based method and needs to consume more time to search for a solution at each iteration. Despite that, the convergence time of the ASR-based method is much shorter than that of the TR-based method since it takes the ASR-based method a few iterations to achieve a small tolerance lower than the preset threshold. When applying Strategy 2, the maximum durations of computation time for the ASR-based method to find the suboptimal solutions are, respectively, 92s, 130s, and 260s under the three damage scenarios. The selected tolerance values by applying Strategy 2 are represented by the red squares in Figures 6, 12, and 18. In terms of convergence time, the proposed method is about ten times faster than the TR-based approach. It is because the TR-based method converges slowly and demands a large number of iterations (e.g., 200) to obtain good results.

Further, the accuracy of the optimal solution selected by using Strategy 1 and that of the suboptimal solution obtained by adopting Strategy 2 are compared and listed in Table 4 when the ASR-based method is applied. For the DS1 scenario, the optimal solutions selected by using Strategy 1 indicate the element E12 with 20%, 19.60%, and 18.80% stiffness reduction in the three cases with different noise levels, while the suboptimal solutions found by using Strategy 2 indicate the element E12 with 20%, 19.68%, and 18.80% damage in the same cases. For the DS2 scenario, the optimal solutions selected by using Strategy 1 include the element E12 with 20%, 19.70%, and 19.15% stiffness reduction and the element E20 with 15%, 15.07%, and 15.36% stiffness reduction in the three cases with different noise levels. The suboptimal solutions found by using Strategy 2 include the element E12 with 20%, 19.72%, and 19.31% damage and the element E20 with 15%, 15.06%, and 15.23% damage in the same cases. For the DS3 scenario, the optimal solutions selected by using Strategy 1 include the element E12 with 20%, 19.89%, and 19.60% damage, the element E20 with 15%, 15.94%, and 17.08% damage, and the element E21 with 20%, 19.17%, and 18.24% damage. The suboptimal solutions found by using Strategy 2 include the element E12 with 20%, 19.88%, and 19.70% damage, the element E20 with 15%, 15.93%, and 17.06% damage, and the element E21 with 20.02%, 19.18%, and 18.18% damage, respectively, under the different noise levels. It is demonstrated that the identified damage locations and severities in the suboptimal solutions and those in the optimal solutions have approximately equal accuracy, and searching for suboptimal solutions consumes much less computation time.

4.2. The Performance Analysis of Adaptive Sparse Regularization Factor. By analyzing the changes in the numerator and denominator of the adaptive regularization factor in equation (12), we can understand how the proposed ASR-based method automatically adapts to different damage scenarios and noise conditions. At the beginning of the iterative updating, the parameters (i.e., $\mathbf{S}^k\Delta\boldsymbol{\alpha}^{k+1}$, $\mathbf{V}_{pq}^c$ in $\Delta\mathbf{V}_{pq}^k = \mathbf{V}_{pq}^m - (\mathbf{V}_{pq}^c)^k$, and $\|\sum\Delta\boldsymbol{\alpha}^{k+1}\|_1$) do not have much difference under different damage scenarios and noise levels. The major variation in the adaptive regularization factor results from $\mathbf{V}_{pq}^m$. Compared with the influence of noise levels, the increase in damage has a dominant influence on $\mathbf{V}_{pq}^m$, so the adaptive regularization factor may increase with the increase in damage. After convergence, the numerator is minimized, and the denominator approaches the real damage situation. With the increase of damage in the three damage scenarios, the denominator increases, and thus the adaptive regularization factor should decrease. It is expected that the adaptive regularization factor in DS1 is larger than that in DS2, and the adaptive regularization factor in DS2 is larger than that in DS3 when subjected to the same noise level. In the three damage scenarios with 0% noise, the numerator is minimized and close to zero, so the adaptive regularization factor probably gets close to zero in the three damage scenarios, and the expected decrease in λ^* with the increase in damage is probably too small to be seen. In all the damage scenarios with 5% noise, the value of the minimized numerator does not have much difference while the denominator increases with the increase of damage, leading to the reduction of λ^*. Similarly, λ^* reduces with the involvement of more damages in all the damage scenarios with 10% noise. With the increase of noise level in each damage scenario, the value of the minimized numerator ascends while the denominator is almost the same, which results in the rising of λ^*.

The theoretical analysis above is found to be consistent with the statistics in Table 5, and these statistics are obtained from the curves of the adaptive regularization factor in Figure 8(b) for DS1, Figure 14(b) for DS2, and Figure 20(b) for DS3. In other words, the numerical results validate the theoretical analysis of the adaptive regularization factor in (12). The influence of the variation in λ^* on damage detection solution can be found in the theoretical analysis in the last paragraph of Section 2.2 and verified by the numerical results in Figure 7(b) for DS1, Figure 13(b) for DS2, and Figure 19(b) for DS3. Both the theoretical analysis and the numerical results demonstrate that the proposed method

Table 4: Comparison of damage identification results of the ASR-based method by using different strategies.

Scenario	Noise level (%)	Identified damage (strategy 1; strategy 2)			Maximum false alarm (%)
		E12 (%)	E20 (%)	E21 (%)	
DS1	0	20.00; 20.00	—	—	—
	5	19.60; 19.68	—	—	0.18; 0.16
	10	18.80; 18.80	—	—	0.84; 0.84
DS2	0	20.00; 20.00	15.00; 15.00	—	—
	5	19.70; 19.72	15.07; 15.06	—	0.15; 0.17
	10	19.15; 19.31	15.36; 15.23	—	0.05; 0.19
DS3	0	20.00; 20.00	15.00; 15.00	20.00; 20.02	-; 0.59
	5	19.89; 19.88	15.94; 15.93	19.17; 19.18	0.06; 0.05
	10	19.60; 19.70	17.08; 17.06	18.24; 18.18	—

Table 5: Comparison of the adaptive regularization factors in different damage scenarios with different noise levels.

Scenario	Noise level (%)	Adaptive regularization factor λ^*	
		At the 1st iteration	After convergence
DS1	0	About 0.61	Close to 0
	5		0.06–0.12
	10		0.11–0.24
DS2	0	About 1.45	Close to 0
	5		0.04–0.07
	10		0.08–0.13
DS3	0	About 3.33	Close to 0
	5		0.03–0.06
	10		0.06–0.11

can automatically adapt to different damage scenarios and noise levels due to the adaptive change in the regularization factor.

4.3. The Analysis of Model Error Influence on ASR-Based Method. To further examine the robustness and accuracy of the ASR-based method, model error is introduced into the different damage scenarios with 10% measurement noise. The model error is simulated with a normally distributed random variation added to the material elasticity modulus vector of the structural elements, and it is expressed as follows:

$$\mathbf{E}_{\text{err}} = \boldsymbol{\varepsilon}_e \mathbf{E}_0, \tag{15}$$

where $\mathbf{E}_0$ and $\mathbf{E}_{\text{err}}$ with the subscripts 0 and err, respectively, represent the vector of the original elasticity modulus of the structural elements and the vector of elasticity modulus of the structural elements with random model error, ε_e with the subscript e denotes a normally distributed random model error vector. Considering the material property is relatively a stable, 1% model error is added to the original elasticity modulus for damage detection investigation. The model error vector ε_e has a mean value equal to unity and a standard deviation equal to 0.01.

The ASR-based method is applied to the damage detection in the presence of 10% noise and 1% model error, and suboptimal solutions are obtained by using Strategy 2 with the threshold value of 10^{-3}. The evolutions of iterative damage identification results are shown in Figure 21, and the identified suboptimal solutions are compared with the preset damage in Figure 22 and Table 6 in the three damage scenarios. For the DS1 scenario, it is noted in Figure 21(a) that the curve of E12 quickly converges to a stable value within the first 5 iterations, and meanwhile, the other curves converge to small values. The suboptimal solution is obtained at the 46th iteration, which is plotted in Figure 22(a) and listed in Table 6. The identified result indicates the element E12 with 19.83% stiffness reduction, which is highly consistent with the preset damage in E12 with 19.26% stiffness reduction, and four notable false alarms are observed in E23, E11, E20, and E18 with 4.36%, 3.55%, 2.08%, and 1.01% stiffness reduction, respectively. For the DS2 scenario, it is found in Figure 21(b) that the damage detection process has a fast convergence within the first 5 iterations, and the results are featured by correct identification of damage locations, satisfactory accuracy in severity identification, and a few false alarms. The features of these results are similar to those in Figure 21(a) for the DS1 scenario. The identified result obtained at the 25th iteration includes the element E12 with 19.55% damage and the element E20 with 18.57% damage, which are compared with the preset damage in E12 and E20 with 19.26% and 13.12% stiffness reduction in Figure 22(b) and Table 6. Only two notable false alarms happen to E11 and E24 with 3.81% and 3.08% stiffness reduction, respectively. For the DS3 scenario, it is observed in Figure 21(c) that the damage detection process has a fast convergence within the first 10 iterations, and the results are featured by correct identification of damage locations, acceptable accuracy in severity

Table 6: The comparison of the preset and identified damages in three different damage scenarios with 10% noise and 1% model error.

Element No.	Scenario					
	DS1		DS2		DS3	
	Preset damage (%)	Identified damage (%)	Preset damage (%)	Identified damage (%)	Preset damage (%)	Identified damage (%)
1	0.86	0.00	0.86	0.00	0.86	0.00
2	0.09	0.00	0.09	0.00	0.09	0.00
3	−0.85	0.00	−0.85	0.00	−0.85	0.00
4	0.87	0.00	0.87	0.00	0.87	0.00
5	−0.44	0.00	−0.44	0.00	−0.44	0.00
6	−0.43	0.50	−0.43	0.74	−0.43	0.95
7	−1.10	0.00	−1.10	0.00	−1.10	0.00
8	0.40	0.00	0.40	0.00	0.40	0.00
9	−0.97	0.00	−0.97	0.00	−0.97	0.00
10	0.17	0.00	0.17	0.00	0.17	0.00
11	−1.97	***3.55***	−1.97	***3.81***	−1.97	***4.15***
12	**19.26**	*19.83*	**19.26**	*19.55*	**19.26**	*19.45*
13	−0.55	0.00	−0.55	0.00	−0.55	0.00
14	−0.82	0.00	−0.82	0.00	−0.82	0.00
15	1.11	0.00	1.11	0.00	1.11	0.00
16	−0.62	0.00	−0.62	0.26	−0.62	0.00
17	−0.26	0.00	−0.26	0.00	−0.26	0.00
18	−0.27	***1.01***	−0.27	0.00	−0.27	***5.03***
19	−1.67	0.00	−1.67	0.00	−1.67	0.00
20	−1.88	***2.08***	**13.12**	*18.57*	**13.12**	*9.07*
21	0.58	0.00	0.58	0.00	**20.58**	*26.15*
22	−0.87	0.00	−0.87	0.00	−0.87	0.00
23	−2.12	***4.36***	−2.12	0.00	−2.12	0.00
24	−0.96	0.00	−0.96	***3.08***	−0.96	0.00
25	0.21	0.00	0.21	0.00	0.21	0.00
26	0.48	0.00	0.48	0.00	0.48	0.00
27	0.10	0.00	0.10	0.00	0.10	0.00
28	0.30	0.00	0.30	0.00	0.30	0.00
29	0.57	0.00	0.57	0.00	0.57	0.00
30	−1.62	0.37	−1.62	0.33	−1.62	0.00
31	0.64	0.00	0.64	0.00	0.64	0.00
32	0.68	0.00	0.68	0.00	0.68	0.00
33	0.01	0.00	0.01	0.00	0.01	0.00
34	−1.30	0.00	−1.30	0.00	−1.30	0.00
35	−1.29	0.00	−1.29	0.00	−1.29	0.00
36	0.81	0.00	0.81	0.00	0.81	0.00
37	0.84	0.00	0.84	0.00	0.84	0.00
38	1.42	0.00	1.42	0.00	1.42	0.00
39	−0.99	0.00	−0.99	0.00	−0.99	0.00
40	−1.18	0.00	−1.18	0.00	−1.18	0.00

*Note: the bold, italics, and bold and italics fonts in the table, respectively, represent the preset real damages, correctly identified damages, and false alarms.

identification, and a few false alarms. These features are similar to those in Figure 21(a) of DS1 and Figure 21(b) of DS2, though the performance in this scenario is not as good as those in DS1 and DS2. The identified result obtained at the 21st iteration includes the element E12 with 19.45% damage, the element E20 with 9.07% damage, and the element E21 with 26.15% damage, and they are compared with the preset damages in E12, E20, and E21 with 19.26%, 13.12%, and 20.58% stiffness reduction in Figure 22(c) and Table 6. Two notable false alarms happen to E18 and E11 with 5.03% and 4.15% stiffness reduction, respectively. To sum up, although more false alarms are observed due to the introduction of model error, the proposed method can still realize fast convergence, correct identification of damage locations, and acceptable accuracy in severity identification in multiple damage scenarios. Moreover, it is noticed in Table 6 that most of the preset damages are ascribed to the model error rather than real damage, and the identified results for those undamaged elements converge to zeros except for a limited number of elements with false alarms induced by measurement noise and model error. This remarkable feature reveals the enhanced sparsity and good model-error resistance of the proposed method.

The curves of the adaptive regularization factors for the different damage scenarios are illustrated in Figure 23 for comparison. The proposed adaptive regularization factors in the case of 10% noise and 1% model error witness a drastic decrease at the first few iterations and then converge to

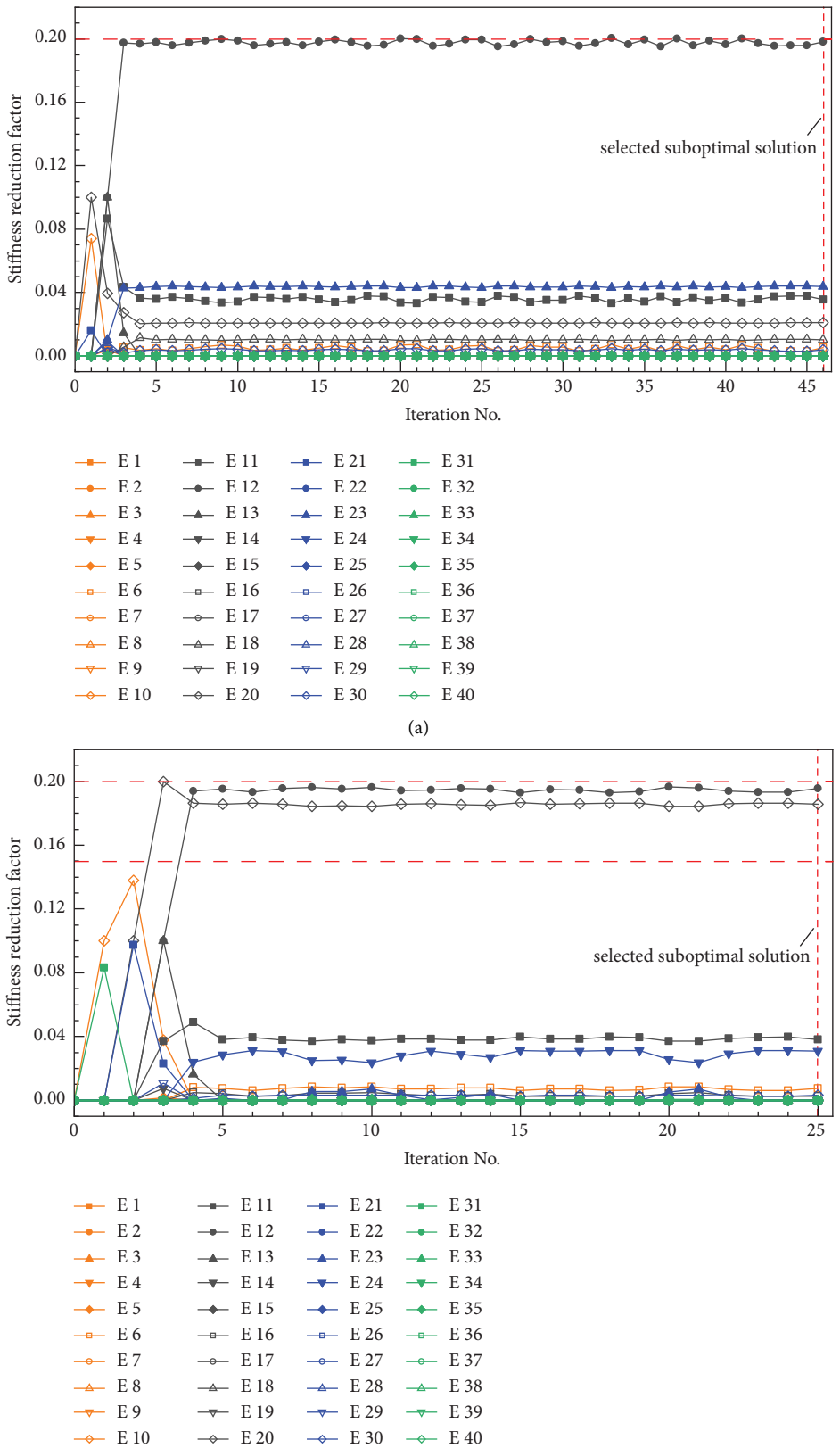

Figure 21: Continued.

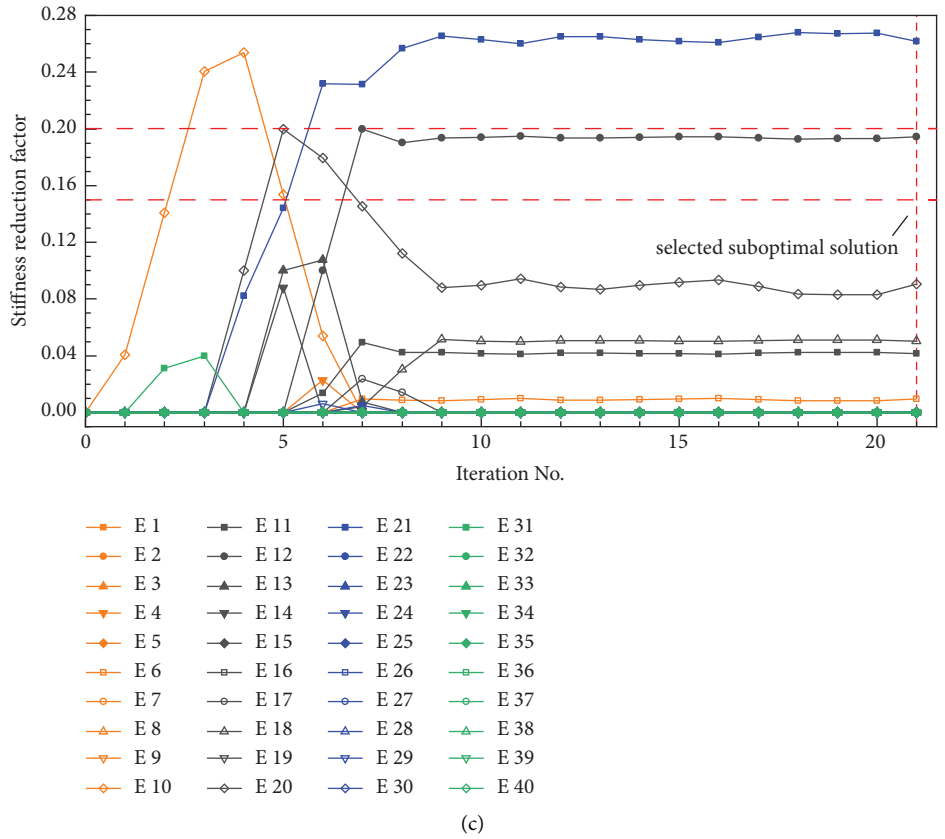

(c)

Figure 21: The evolution of iterative damage identification results of different damage scenarios by using the ASR-based method in the situation of 10% noise and 1% model error. (a) The solution of DS1. (b) The solution of DS2. (c) The solution of DS3.

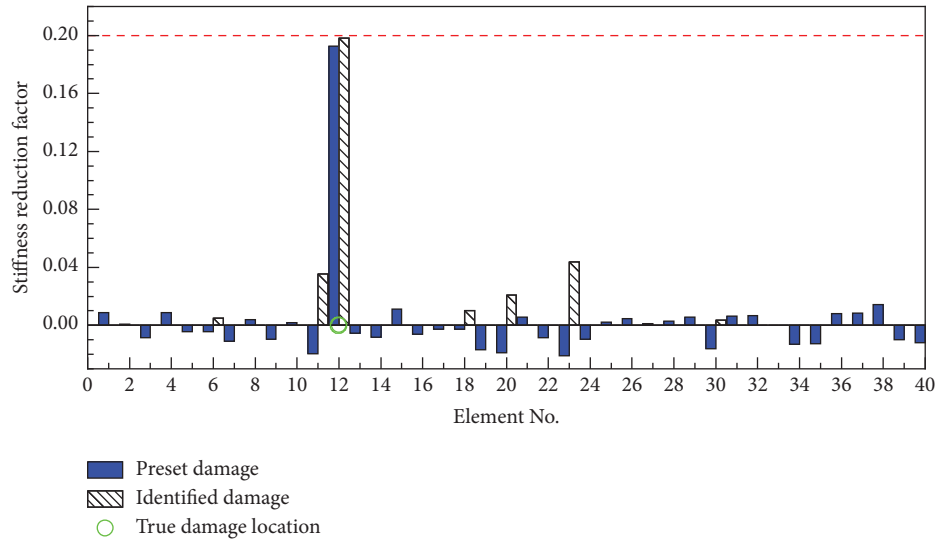

(a)

Figure 22: Continued.

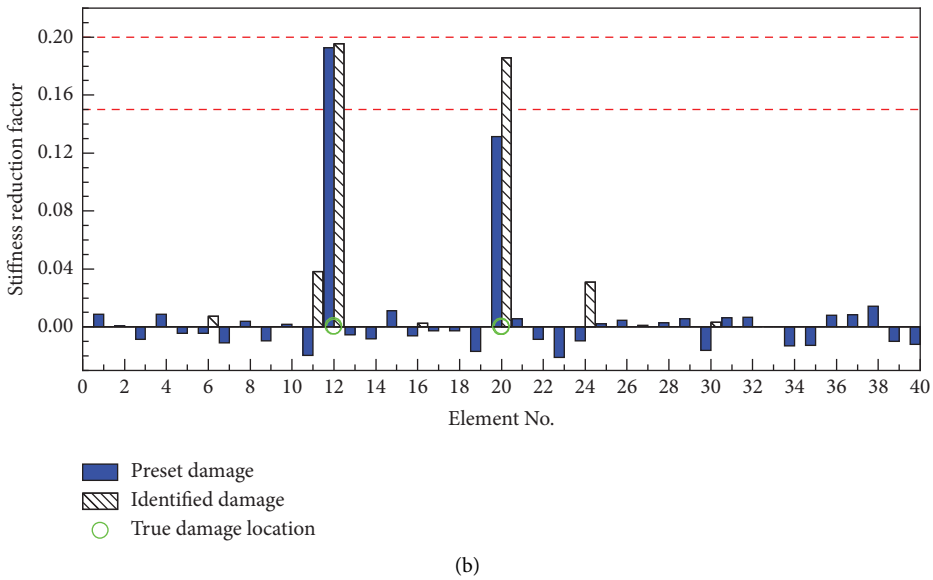

(b)

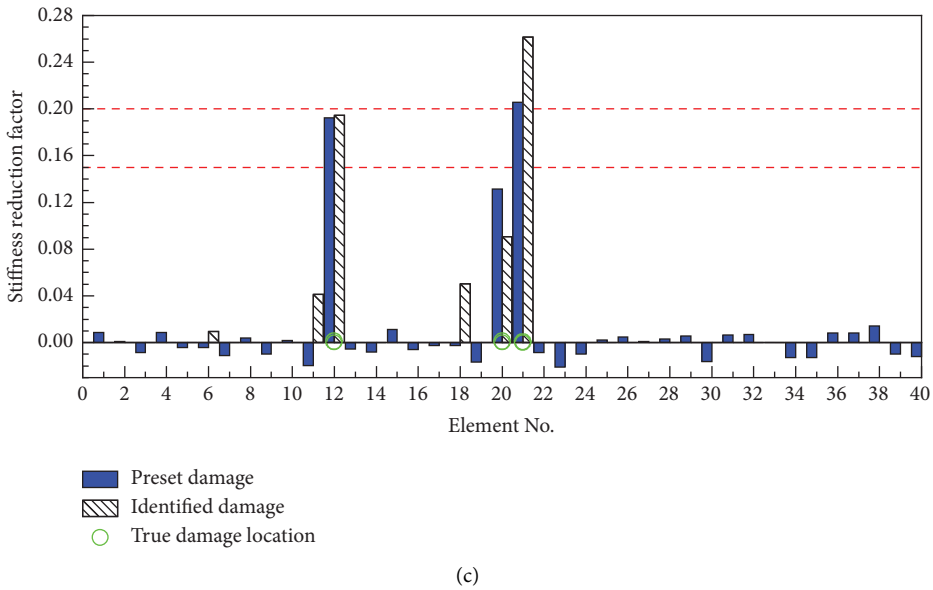

(c)

Figure 22: The comparison between the preset damage and the identified damage by using the ASR-based method in the situation of 10% noise and 1% model error. (a) The suboptimal solution of DS1. (b) The suboptimal solution of DS2. (c) The suboptimal solution of DS3.

stable values with slight fluctuation in amplitude. Specifically, the proposed regularization factors have a sharp reduction from 1.04, 2.13, and 4.41 at the 1st iteration for DS1, DS2, and DS3, respectively, to small values, i.e., the small value with slight fluctuation within 0.07–0.14 for DS1, the small value with slight fluctuation within 0.06–0.10 for DS2, and the small value with slight fluctuation within 0.05–0.07 for DS3. The initial value of the adaptive regularization factor is larger in the scenario with more damages, and this can be ascribed to the larger difference between the intact model and the damaged structure induced by more damages. After convergence, a smaller adaptive factor can be automatically achieved when more damages are involved, which is consistent with the bigger solution norms obtained in the scenario with more damages. This implies that the automatically determined adaptive regularization factor can effectively adjust the sparsity constraint for achieving better multidamage detection performance in the complex multidamage scenario with measurement noise and model error.

4.4. The Analysis of Sensor Number Influence on ASR-Based Method. The l_1-regularization techniques generally have the advantage of solving the damage detection problem by using a small number of sensors. To investigate the sensor number influence on the ASR-based method, the damage detection studies with 6 and 4 optimally placed sensors are further conducted and compared with the previous damage detection study with 8 optimally placed sensors. The optimal sensor configurations with 6 and 4 sensors, as shown in Figures 2(b) and 2(c), are determined by conducting the EfI optimal sensor placement with the first 6 and 4 modes

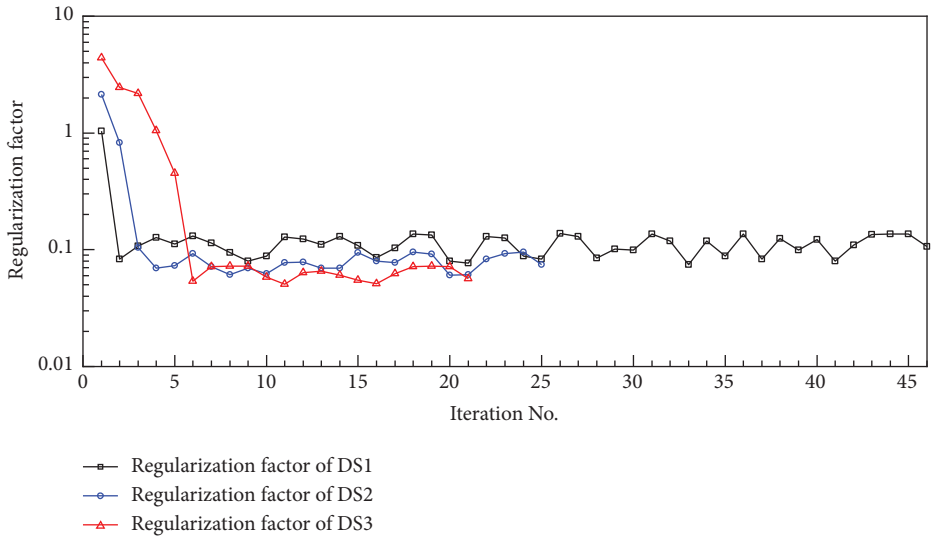

Figure 23: The curves of the adaptive regularization factor for three damage scenarios in the situation of 10% noise and 1% model error.

Table 7: Comparison of damage identification results of the ASR-based method by using different numbers of sensors.

Scenario	Sensor number	Preset damage (%)			Identified damage (%)			Maximum false alarm (%)
		E12	E20	E21	E12	E20	E21	
DS1	8	19.26	—	—	19.83	—	—	4.36
	6				20.07	—	—	4.25
	4				19.58	—	—	3.63
DS2	8	19.26	13.12	—	19.55	18.57	—	3.81
	6				19.67	18.53	—	3.67
	4				19.76	18.05	—	3.51
DS3	8	19.26	13.12	20.58	19.45	9.07	26.15	5.03
	6				19.82	0.00	27.57	11.16
	4				19.33	0.00	27.96	10.55

considered, respectively. The ASR-based method is applied to the damage detection under the three damage scenarios with the different sensor numbers in the situation of 10% noise and 1% model error. For the cases with the reduced numbers of sensors, the damage detection results are obtained by setting the threshold value as 10^{-3} and the maximum iteration number as 50. In the three damage scenarios, the identified suboptimal solutions of the cases using 8, 6, and 4 sensors are compared with the preset damage in Figure 24 and Table 7. For the DS1 scenario, the suboptimal solution is plotted in Figure 24(a). The identified results indicate the element E12 with 19.83%, 20.07%, and 19.58% stiffness reduction, respectively, when using 8, 6, and 4 sensors, which are consistent with the preset damage in E12 with 19.26% stiffness reduction. The maximum false alarms are 4.36% (E23), 4.25% (E23), and 3.63% (E22) stiffness reduction in the cases with different sensor numbers. For the DS2 scenario, the identified results include the element E12 with 19.55%, 19.67%, and 19.76% stiffness reduction and the element E20 with 18.57%, 18.53%, and 18.05% stiffness reduction, respectively, when using 8, 6, and 4 sensors. They are compared with the preset damage in E12 with 19.26% and that in E20 with 13.12% stiffness reduction in Figure 24(b) and Table 7. The maximum false alarms when using the different numbers of sensors are 3.81% (E11), 3.67% (E11), and 3.51% (E11) stiffness reduction, respectively. For the DS3 scenario, the identified results include the element E12 with 19.45%, 19.82%, and 19.33% stiffness reduction, the element E20 with 9.07%, 0.00%, and 0.00% stiffness reduction, and the element E21 with 26.15%, 27.57%, and 27.96% stiffness reduction, respectively, when using 8, 6, and 4 sensors, which are compared with the preset damages in E12, E20, and E21 with 19.26%, 13.12%, and 20.58% stiffness reduction in Figure 24(c) and Table 7. The identified maximum false alarms when using the different numbers of sensors are 5.03% (E18), 11.16% (E19), and 10.55% (E19) stiffness reduction, respectively. In the DS1 and DS2 scenarios featured by isolated damage, it is noted that the ASR-based method can reach similar identification results when the number of sensors is reduced, and the damage locations and severities can be satisfactorily identified under the coupling contamination of measurement noise and model error. In the DS3 scenario with isolated damage and a grouped damage, the isolated damage in E12 can be accurately detected when using the different numbers of sensors while the same identification performance does not occur to the grouped damage in E20 and E21. Specifically, the damage in E21 can be acceptably identified when

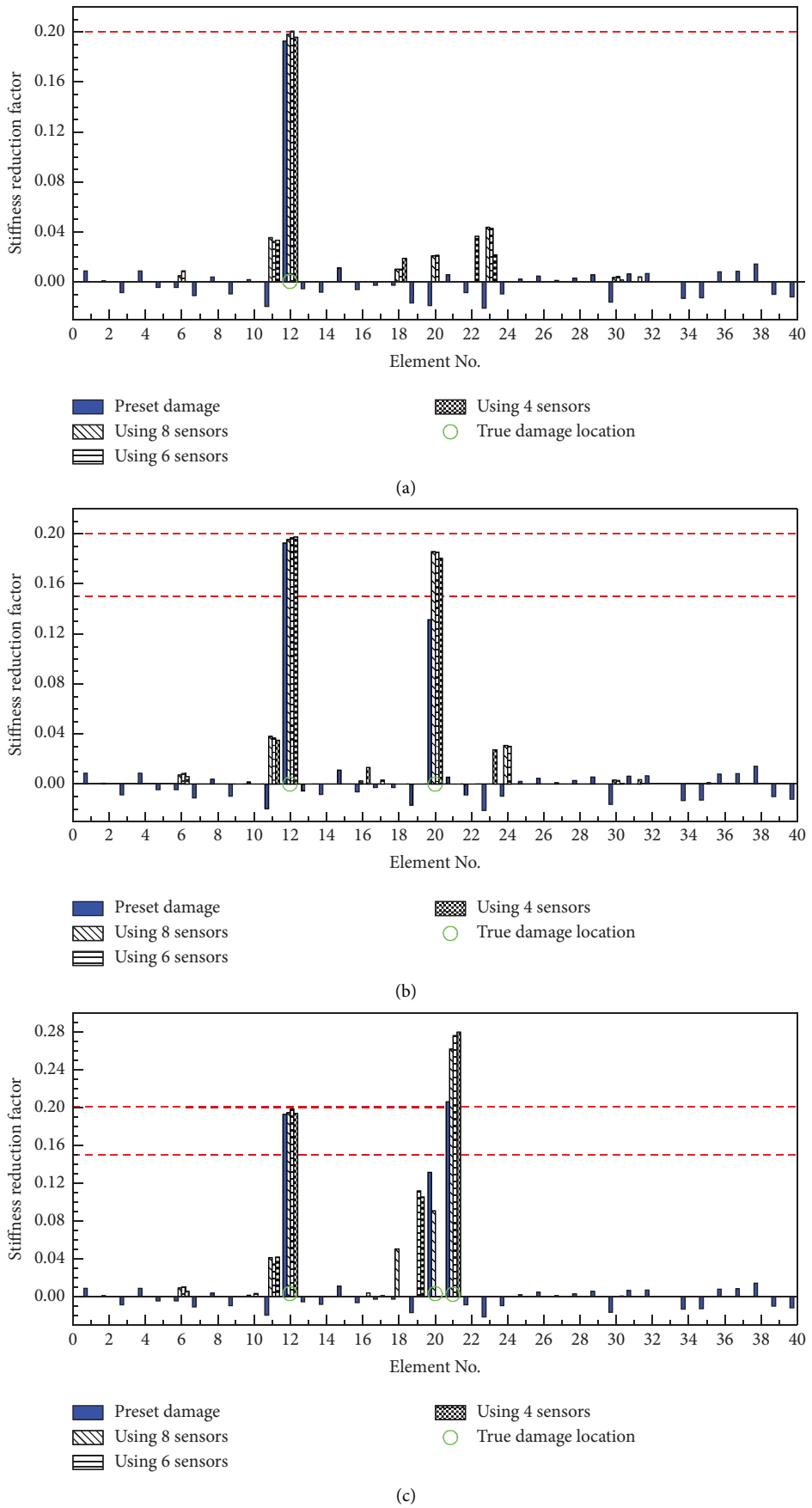

FIGURE 24: The comparison of damage detection results obtained by using the ASR-based method with the different sensor numbers in the situation of 10% noise and 1% model error. (a) The suboptimal solutions of DS1. (b) The suboptimal solutions of DS2. (c) The suboptimal solutions of DS3.

the sensor number is reduced, the damage in E20 can be acceptably identified by using the optimal sensor configuration with 8 sensors rather than using the configurations with 6 and 4 sensors, and the false alarms happen to the adjacent element E19. This analysis has demonstrated that the reduction of the sensor number to 6 or 4 in the optimal sensor configuration has a minor effect on the correct identification of isolated damage while the identification performance of grouped damage becomes worse due to the lack of modal information and decreased identification ability.

5. Conclusions

An adaptive sparse regularization method has been proposed for tackling the ill-posed inverse problem of structural damage detection using a small number of optimally placed sensors. This method is governed by the response covariance-based cost function, which consists of the l_2-norm objective of residue for assuring data fidelity and the l_1-norm regularization term of solution for taking into account the sparsity of local damage. Different from traditional cost functions, it is proposed to use the accumulated stiffness reduction rather than the one-step adjustment of stiffness reduction in the sparse regularization term. The sparse constraint to the accumulated stiffness reduction enhances both the sparsity of the final solution and the flexibility of one-step adjustment. Rather than using subjective or empirical selection strategies for assigning a value to the l_1-regularization factor, the adaptive regularization factor is mathematically derived by assuming the residue norm and solution norm are equally important for damage detection. Since the l_1-regularization method lacks a closed-form solution, a predictor-corrector primal-dual path-following algorithm is introduced to efficiently and robustly search for optimal damage identification solutions on the proposed cost function.

The numerical experiment and the comparative study with the widely used TR-based method reveal the effectiveness and outperformance of the proposed ASR-based method under different damage scenarios with various noise levels. It has been demonstrated that the proposed method is advantageous in several aspects, including high accuracy with few false alarms, a stable iterative process, and fast convergence. Moreover, it is noted that the proposed adaptive l_1-regularization factor can automatically and adaptively adjust the tradeoff between the residue norm and the solution norm, thereby facilitating accurate identification of the damage locations and severities in different damage and noise conditions. In addition, the damage detection solutions of the proposed method can converge to stable values quickly, which enables a preset small threshold of the two tolerances to determine the accurate solutions and automatically terminate the searching process. Besides, it is demonstrated that the proposed ASR-based method has good model-error resistance ability, which helps achieve satisfactory damage detection results in the different damage scenarios with coupled noise and model error. Finally, the sensor number influence on the proposed ASR-based method in the situation of coupled noise and model error has also been analyzed. It is found that the reduction of sensor number to a smaller amount in the optimal sensor configuration has a minor effect on the correct identification of isolated damage, while the identification performance of grouped damage becomes worse due to the lack of modal information and decreased identification ability.

Symbols

$\mathbf{C}$: The damping matrix
$C_{pq}(\tau)$: The normalized cross-covariance function computed from the sensors p and q
$\mathbf{d}$: The displacement response vector
$\dot{\mathbf{d}}$: The velocity response vector
$\ddot{\mathbf{d}}$: The acceleration response vector
$\ddot{\mathbf{d}}_p(t)$, $\ddot{\mathbf{d}}_q(t)$: The acceleration response recorded by the sensor p or q
$\hat{\ddot{\mathbf{d}}}_p(t)$, $\hat{\ddot{\mathbf{d}}}_q(t)$: The normalized acceleration response recorded by the sensor p or q
$\ddot{\mathbf{d}}^m$: The noise polluted acceleration response measured from the damaged structure
$\ddot{\mathbf{d}}^c$: The calculated acceleration response of the damaged structure without noise
$\mathrm{diag}(\cdot)$: The diagonal elements of the matrix
$\mathrm{E}[\cdot]$: The expectation operation
$\mathbf{EI}$: The independence contribution vector
$\mathbf{E}_0$: The vector of the original elasticity modulus of the structural elements
$\mathbf{E}_{\mathrm{err}}$: The vector of the elasticity modulus of the structural elements with random model error
$\mathbf{F}$: The excitation force vector
$\mathbf{K}$: The global stiffness matrix
$\mathbf{K}^d$: The global stiffness matrix of the damaged structure
$\mathbf{K}_i$: The stiffness matrix of the i^{th} element
$\mathbf{L}_{\mathbf{F}}$: The mapping matrix relating the excitation force to specific DOFs of the structure
$\mathbf{M}$: The global mass matrix
$\mathrm{N_p}$: The noise level
$\mathbf{N}_{\mathrm{oise}}$: The standard normal distribution vector with zero mean and unit standard deviation
ne: The total element number of the structure
nt: The total number of time lags
$\mathbf{S}$: The sensitivity matrix of the damage index vector to the fractional stiffness change vector
$\mathrm{std}(\cdot)$: The standard deviation operator
t: The time variable
$\mathrm{Tol1}(k)$, $\mathrm{Tol2}(k)$: The two tolerances at the k^{th} iteration
$\mathbf{V}_{pq}$: The response covariance-based damage index vector
$\mathbf{V}_{pq}^m$: The response covariance-based damage index vector computed from the measured responses
$\mathbf{V}_{pq}^c$:

The response covariance-based damage index vector computed through the response of the FE model

$\Delta \mathbf{V}_{pq}$: The vector of the difference between $\mathbf{V}_{pq}^{\mathbf{m}}$ and $\mathbf{V}_{pq}^{\mathbf{c}}$

α_i: The coefficient of stiffness matrix corresponding to the i^{th} element

α: The coefficient vector of the stiffness matrix

$\Delta\alpha_i$: The fractional change in stiffness of the i^{th} element

$\Delta\alpha$: The vector of the accumulated stiffness change

$\Delta\alpha^k$: The fractional stiffness change vector at the k^{th} iteration

$\Delta\alpha_{\text{r}}^{k+1}$: The estimated stiffness reduction at the $(k+1)^{\text{th}}$ iteration for calculating the adaptive regularization factor λ^*

$\sum(\Delta\alpha^k)$: The accumulated stiffness reduction vector of the previous k iterations

ε_e: The vector of normally distributed random model error

λ: The regularization factor of the Tikhonov regularization

λ^*: The adaptive regularization factor of the adaptive sparse regularization

ξ_1, ξ_2: The first two damping ratios of Rayleigh damping

σ_p^0, σ_q^0: The standard deviation of the $\ddot{\mathbf{d}}_p$ or $\ddot{\mathbf{d}}_q$ recorded from the intact structure

τ: The time lag

Φ: The mode shape matrix

$(\cdot)^0$: The superscript 0 denotes the parameter from the initial state

$(\cdot)^c$: The superscript c denotes the parameter calculated by using the finite element model

$(\cdot)^d$: The superscript d denotes the parameter under the state of damage

$(\cdot)_i$: The subscript i denotes the element number

$(\cdot)^k$: The superscript k denotes the iteration number

$(\cdot)^m$: The superscript m denotes the parameter obtained from measurement

$(\cdot)_{pq}$: The subscript pq denotes the parameter obtained from the sensors p and q

$(\cdot)_s$: The subscript s denotes the total number of the sensors

Abbreviations

ASR: Adaptive sparse regularization
DOFs: Degrees of freedom
DS1: Damage scenario 1
DS2: Damage scenario 2
DS3: Damage scenario 3
EfI: Effective independence
FE: Finite element
LASSO: Least absolute shrinkage and selection operator
TR: Tikhonov regularization.

Data Availability

The data used to support the findings of this study are included in the article.

Conflicts of Interest

The authors declare that they have no conflicts of interest.

Authors' Contributions

Jian-Fu Lin and Wei-Lin Wu contributed equally to this work.

Acknowledgments

The authors acknowledge the support from the China Earthquake Administration's Science for Earthquake Resilience Project (Grant no. XH204702), the National Key R&D Program of China (Grant nos. 2019YFB2102700 and 2019YFC1511005-05), National Natural Science Foundation of China (Grant no. 52008258), Shenzhen Science and Technology Program (Grant no. KQTD20180412181337494), and Shenzhen Key Laboratory of Structure Safety and Health Monitoring of Marine Infrastructures (In preparation, Grant no. ZDSYS20201020162400001).

References

[1] S. W. Doebling, C. R. Farrar, and M. B. Prime, "A summary review of vibration-based damage identification methods," *The Shock and Vibration Digest*, vol. 30, no. 2, pp. 91–105, 1998.

[2] E. P. Carden and P. Fanning, "Vibration based condition monitoring: a Review," *Structural Health Monitoring*, vol. 3, no. 4, pp. 355–377, 2004.

[3] R. R. Hou and Y. Xia, "Review on the new development of vibration-based damage identification for civil engineering structures: 2010–2019," *Journal of Sound and Vibration*, vol. 491, Article ID 115741, 2021.

[4] X. Y. Li and S. S. Law, "Matrix of the covariance of covariance of acceleration responses for damage detection from ambient vibration measurements," *Mechanical Systems and Signal Processing*, vol. 24, no. 4, pp. 945–956, 2010.

[5] S. S. Law, J. F. Lin, and X. Y. Li, "Structural condition assessment from white noise excitation and covariance of covariance matrix," *AIAA Journal*, vol. 50, no. 7, pp. 1503–1512, 2012.

[6] S. S. Law and J. F. Lin, "Unit impulse response estimation for structural damage detection under planar multiple excitations," *Journal of Applied Mechanics*, vol. 81, no. 2, Article ID 021015, 2013.

[7] J. F. Lin and Y. L. Xu, "Two-stagecovariance-based multi-sensing damage detection method," *Journal of Engineering Mechanics*, vol. 143, no. 3, Article ID B4016003, 2017.

[8] J. F. Lin and Y. L. Xu, "Response covariance-based sensor placement for structural damage detection," *Structure and Infrastructure Engineering*, vol. 14, no. 9, pp. 1207–1220, 2018.

[9] J. F. Lin, Y. L. Xu, and S. S. Law, "Structural damage detection-orientedmulti-type sensor placement with multi-objective

optimization," *Journal of Sound and Vibration*, vol. 422, pp. 568–589, 2018.

[10] H. P. Wan and Y. Q. Ni, "Bayesian modeling approach for forecast of structural stress response using structural health monitoring data," *Journal of Structural Engineering*, vol. 144, no. 9, Article ID 04018130, 2018.

[11] H. P. Wan and Y. Q. Ni, "Bayesian multi-task learning methodology for reconstruction of structural health monitoring data," *Structural Health Monitoring*, vol. 18, no. 4, pp. 1282–1309, 2019.

[12] J. F. Lin, Y. L. Xu, and S. Zhan, "Experimental investigation on multi-objectivemulti-type sensor optimal placement for structural damage detection," *Structural Health Monitoring*, vol. 18, no. 3, pp. 882–901, 2019.

[13] J. F. Lin, J. F. Wang, L. X. Wang, and S. S. Law, "Structural damage diagnosis-oriented impulse response function estimation under seismic excitations," *Sensors*, vol. 19, no. 24, p. 5413, 2019.

[14] Y. L. Xu, J. F. Lin, S. Zhan, and F. Y. Wang, "Multi-stage damage detection of a transmission tower: numerical investigation and experimental validation," *Structural Control and Health Monitoring*, vol. 26, Article ID e2366, 2019.

[15] X. Y. Li, S. J. Lin, S. S. Law, Y. Z. Lin, and J. F. Lin, "Fusion of structural damage identification results from different test scenarios and evaluation indices in structural health monitoring," *Structural Health Monitoring*, vol. 10, 2020.

[16] D. Calvetti, S. Morigi, L. Reichel, and F. Sgallari, "Tikhonov regularization and the L-curve for large discrete ill-posed problems," *Journal of Computational and Applied Mathematics*, vol. 123, no. 1-2, pp. 423–446, 2000.

[17] B. Titurus and M. I. Friswell, "Regularization in model updating," *International Journal for Numerical Methods in Engineering*, vol. 75, no. 4, pp. 440–478, 2008.

[18] B. Weber, P. Paultre, and J. Proulx, "Consistent regularization of nonlinear model updating for damage identification," *Mechanical Systems and Signal Processing*, vol. 23, no. 6, pp. 1965–1985, 2009.

[19] X. Y. Li and S. S. Law, "Adaptive Tikhonov regularization for damage detection based on nonlinear model updating," *Mechanical Systems and Signal Processing*, vol. 24, no. 6, pp. 1646–1664, 2010.

[20] H. P. Zhu, L. Mao, and S. Weng, "A sensitivity-based structural damage identification method with unknown input excitation using transmissibility concept," *Journal of Sound and Vibration*, vol. 333, no. 26, pp. 7135–7150, 2014.

[21] Y. Q. Bao, H. Li, and J. P. Ou, "Emerging data technology in structural health monitoring: compressive sensing technology," *J. Civil Struct. Health Monit.,* vol. 4, no. 2, pp. 77–90, 2014.

[22] S. Nagarajaiah and Y. Yang, "Modeling and harnessing sparse and low-rank data structure: a new paradigm for structural dynamics, identification, damage detection, and health monitoring," *Structural Control and Health Monitoring*, vol. 24, no. 1, Article ID e1851, 2017.

[23] S. Zhou, Y. Bao, and H. Li, "Structural damage identification based on substructure sensitivity and l1 sparse regularization. Sensors and Smart Structures Technologies for Civil, Mechanical, and Aerospace Systems," *Civil Structural Health Monitoring Workshop (CSHM-4)*, vol. 8692, 2013.

[24] E. M. Hernandez, "Identification of isolated structural damage from incomplete spectrum information using l_1-norm minimization," *Mechanical Systems and Signal Processing*, vol. 46, no. 1, pp. 59–69, 2014.

[25] X. Q. Zhou, Y. Xia, and S. Weng, "L_1 regularization approach to structural damage detection using frequency data," *Structural Health Monitoring*, vol. 14, no. 6, pp. 571–582, 2015.

[26] Y. H. Wu and X. Q. Zhou, "L_1 regularized model updating for structural damage detection," *International Journal of Structural Stability and Dynamics*, vol. 18, no. 12, Article ID 1850157, 2018.

[27] R. R. Hou, Y. Xia, and X. Zhou, "Structural damage detection based on l_1 regularization using natural frequencies and mode shapes," *Structural Control and Health Monitoring*, vol. 25, no. 3, Article ID e2107, 2018.

[28] R. R. Hou, X. Wang, and Y. Xia, "Sparse damage detection via the elastic net method using modal data," *Structural Health Monitoring*, vol. 21, no. 3, pp. 1076–1092, 2021.

[29] X. Y. Fan, J. Li, H. Hao, and S. L. Ma, "Identification of minor structural damage based on electromechanical impedance sensitivity and sparse regularization," *Journal of Aerospace Engineering*, vol. 31, no. 5, Article ID 04018061, 2018.

[30] Z. G. Yue, Z. P. Chen, and L. Yu, "Comparative studies on structural damage detection using L<SUB align=right>p norm regularisation," *International Journal of Lifecycle Performance Engineering*, vol. 3, no. 2, pp. 171–186, 2019.

[31] Z. W. Luo and L. Yu, "Regularization strategies for contiguous and noncontiguous damage detection of structures," *International Journal of Computational Methods*, vol. 18, no. 6, Article ID 2140001, 2020.

[32] C. D. Zhang and Y. L. Xu, "Comparative studies on damage identification with Tikhonov regularization and sparse regularization," *Structural Control and Health Monitoring*, vol. 23, no. 3, pp. 560–579, 2016.

[33] C. B. Smith and E. M. Hernandez, "Detection of spatially sparse damage using impulse response sensitivity and LASSO regularization," *Inverse Problems in Science and Engineering*, vol. 27, no. 1, pp. 1–16, 2018.

[34] M. El Mountassir, S. Yaacoubi, G. Mourot, and D. Maquin, "Sparse estimation based monitoring method for damage detection and localization: a case of study," *Mechanical Systems and Signal Processing*, vol. 112, pp. 61–76, 2018.

[35] Z. Chen, W. Yang, J. Li, T. Yi, J. Wu, and D. Wang, "Bridge influence line identification based on adaptive B-spline basis dictionary and sparse regularization," *Structural Control and Health Monitoring*, vol. 26, no. 6, Article ID e2355, 2019.

[36] D. Mascarenas, A. Cattaneo, J. Theiler, and C. Farrar, "Compressed sensing techniques for detecting damage in structures," *Structural Health Monitoring*, vol. 12, no. 4, pp. 325–338, 2013.

[37] Y. Yang and S. Nagarajaiah, "Output-only modal identification by compressed sensing: non-uniformlow-rate random sampling," *Mechanical Systems and Signal Processing*, vol. 56-57, pp. 15–34, 2015.

[38] L. Wang and Z. R. Lu, "Sensitivity-free damage identification based on incomplete modal data, sparse regularization and alternating minimization approach," *Mechanical Systems and Signal Processing*, vol. 120, pp. 43–68, 2019.

[39] Z. Lai and S. Nagarajaiah, "Semi-supervised structural linear/nonlinear damage detection and characterization using sparse identification," *Structural Control and Health Monitoring*, vol. 26, no. 3, Article ID e2306, 2018.

[40] D. Malioutov, M. Cetin, and A. S. Willsky, "A sparse signal reconstruction perspective for source localization with sensor arrays," *IEEE Transactions on Signal Processing*, vol. 53, no. 8, pp. 3010–3022, 2005.

[41] R. R. Hou, Y. Xia, Y. Q. Bao, and X. Q. Zhou, "Selection of regularization parameter for l_1-regularized damage detection," *Journal of Sound and Vibration*, vol. 423, pp. 141–160, 2018.

[42] H. Yao, P. Gerstoft, P. M. Shearer, and C. Mecklenbräuker, "Compressive sensing of the Tohoku-Oki Mw 9.0 earthquake: frequency-dependent rupture modes," *Geophysical Research Letters*, vol. 38, no. 20, Article ID L20310, 2011.

[43] R. H. Tütüncü, K. C. Toh, and M. J. Todd, *SDPT3 - a MATLAB Software Package for Semidefinite-Quadratic-Linear Programming, Version 3.0*, Carnegie Mellon University, Pittsburgh, PA, USA, 2001.

[44] D. C. Kammer, "Sensor placement for on-orbit modal identification and correlation of large space structures," *Journal of Guidance, Control, and Dynamics*, vol. 14, no. 2, pp. 251–259, 1991.